Global And Arctic Climate Engineering: Numerical Model Studies

Author

Ernest Agyemang-Oko from Kumasi, Ghana

Matriculation Number: 3184059

Reviewers

Prof. Dr. Gerrit Lohmann

Dr. Christoph Völker

Supervised by

Prof. Dr. Gerrit Lohmann

Dr. Hu Yang

Master Thesis

SUBMITTED IN PARTIAL FULFILMENT OF THE REQUIREMENT OF THE

DEGREE OF MASTER OF SCIENCE IN ENVIRONMENTAL PHYSICS

Institute of Environmental Physics and Remote Sensing (IUP - IFE)

University of Bremen, Bremen, Germany

February 03, 2022

Declaration of Copyright

Name: Ernest Agyemang-Oko Matrikel-Nr.: 3184059

Declaration of honor

I hereby confirm on my honor that I personally prepared the present academic work and carried out myself the activities directly involved with it. I also confirm that I have used no resources other than those declared. All formulations and concepts adopted literally or in their essential content from printed, unprinted or Internet sources have been cited according to the rules for academic work and identified by means of footnotes or other precise indications of source. The support provided during the work, including significant assistance from my supervisors has been indicated in full. The academic work has not been submitted to any other examination office authority. The work is submitted in printed and electronic form. I confirm that the content of the digital version is completely identical to that of the printed version.

Date: February 03, 2022 Ernest Agyemang-Oko

Declaration of publication

I hereby agree, that my thesis will be available for third-party review for the purpose of academic research.

I hereby agree, that my thesis will be available after 30 years in the university archive for third-party review for the purpose of academic research.

I hereby do not agree, that my thesis will be available for third-party review for the purpose of academic research.

Date: February 03, 2022 Ernest Agyemang-Oko

Acknowledgement

I would like to express my deep and sincere gratitude to my research supervisor, Prof. Dr. Gerrit Lohmann, for giving me the opportunity to work under his supervision in the Paleoclimate Dynamics group of Alfred Wegener Institute (AWI). I have benefited immensely from his deep scientific knowledge and it was a great privilege and honor to do my research under his guidance.

I would also like to acknowledge and give my warmest thanks to Dr. Hu Yang for his supervision and tutorship. His guidance and advice carried me through all the stages of writing my thesis and I am extremely grateful to him.

My sincere appreciation to Dr. Christoph Völker, as the second reader of this thesis, for your valuable comments that helped to put this thesis in a better perspective.

Finally, I would like to give special thanks to my family and friends for their continuous support. I thank everyone for the motivation, encouragement, and support through the ups and downs during this Master's thesis.

Abstract

Climate engineering is an intentional large-scale intervention in the Earth's climate system to counteract the anthropogenic warming. It has been proposed and recently gained attention as a potential option for tackling global warming. To evaluate the feasibility and impacts of geoengineering, we performed idealized climate simulations using solar geoengineering scheme by artificially reducing the incoming solar radiation at the top of the atmosphere (TOA) either globally or over the polar regions. Four simulations were conducted, i.e. pre-industrial control simulation, global warming simulation with 4xCO_2, global uniform solar reduction and reduction of solar radiation regionally over both poles. Our results indicate that the 4xCO_2 induced a 6.7 K global mean surface temperature raise, amplified over both poles primarily during the hemisphere winter. Besides, the warming also cause intensification and poleward shift of the global precipitation pattern.
A 4.2% globally uniform solar reduction can largely compensate the global mean warming caused by 4xCO_2. We find that solar reduction is efficient to reduce the warming at the region where the background sunshine is strong, such as the low-latitude summer warming. However, the CO_2 induced warming over high latitudes during winter are less sensitive to solar reduction. The solar reduction leads to more residual warming over land than over the ocean. Therefore, it could result in hemisphere asymmetric residual warming due to the hemisphere asymmetric land-sea distribution. This will eventually cause northward shift of the Intertropical Convergence Zone and the associated low-latitude precipitation pat-

tern. Moreover, we notice that solar reduction could lead to an overall weakening of the global hydrological cycle, suggesting that over reduction of solar radiation may result in large-scale drought.

The CO_2 forcing introduces more warming over the poles than low-latitudes. The ice sheets around both poles are critical for further sea level rise. Our experiments indicate that 16% solar reduction over both poles (higher than 60 °N/S) is able to restore the summer temperature and sea ice extent. However, such polar regional geoengineering leads to stronger and more frequent high-latitude storms. Our simulation results show that Solar Radiation Management is an effective way to offset global mean temperature raise.

Nevertheless, climate engineering by reducing insolation at the TOA, either globally or regionally, have strong impact on the hydrological cycle and the regional climate. In spite of the fact that our climate simulations are being highly idealised, these simulations can provide useful information about the climate respond to scenarios with more realistic GHG forcing.

Contents

List of Figures

List of Tables

Chapter 1

Introduction

Global warming due to emissions have increased and emerged as one of the biggest environmental challenges facing the world. Its effects have been evident for many years and will become more severe in the coming decades. Global warming has enhanced since 1990 and the risks of increased global temperatures are great, as the IPCC's 5th Report shows. In 2015, the Paris Climate Change Agreement by world's countries resolved to strengthen the global response to the threat of climate change by limiting the global average temperature rise to well below 2 ^{o}C and to pursue efforts to limit warming to 1.5 ^{o}C above the pre-industrial level by 2100. Despite this ambition, staying within 2 ^{o}C limit seems extremely unlikely as anthropogenic emissions keeps on increasing. The global average surface temperature has increased by more than 0.8 degrees celsius (0.8 ^{o}C) and global mean sea level has risen by approximately 0.2 m since the pre-industrial era (*Stocker et al.*, 2013), and even more sensitive in polar regions as climate change is manifesting strongest warming there due to rapid CO_2 emissions which have caused a net radiative forcing at the top of the atmosphere (TOA). According to *Lohmann* (2020), global temperature is determined by the radiation budget through the incoming energy from the sun and the outgoing energy from the Earth. The Earth's energy budget is out of balance due to increased atmospheric greenhouse gas concentra-

tions which has profound impacts on the Earth's climate by trapping more heat in the atmosphere. An increase in global temperature will have adverse effects on the Earth as it has already evident, it will change the amount and also the pattern of precipitation. Changes in temperature and precipitation or rainfall patterns increase the frequency, duration and intensity of other extreme weather events. Increasing in ocean heat content, shrinkage in the polar sea ice coverage, decline in glaciers and snow cover are all evidence of changing global climate (*Stocker et al.*, 2013).

Global anthropogenic carbon dioxide emissions from burning fossil fuels have significantly increased since 1900. Greenhouse gas emission growth has been accelerated over the last decades (*Stocker et al.*, 2013). China, the United States, the European Union, India, Russian and Japan were the top carbon dioxide (CO_2) emitters in 2014 Global CO_2 emissions from fossil fuel combustion and some industrial processes. Increasing in greenhouse gas (GHG) emissions are leading to global warming and climate change. Effectively eradicating net greenhouse gas emissions remains the only permanent method of addressing climate change. However, the efforts to mitigate climate change by reducing these emissions are proving to be particularly difficult and challenging. This has led to an interest in climate engineering (*Crutzen*, 2006), which has recently gained attention as a way to manage climate risks as proposed by some scientists, to counteract climate change by artificially cooling the planet.

Climate Engineering (also referred to as Geoengineering), is the intentional large-scale intervention in the Earth's climate system to counteract greenhouse gas-induced warming. Climate engineering has been one of the most rapidly growing areas of climate research as a potential option for tackling global warming to limit climate change. Geoengineering can be broadly divided into two main categories (*Caldeira et al.*, 2013): Solar Radiation Management (SRM) (also called solar geoengineering), which aims to reflect more sunlight to space and Carbon Dioxide

Removal methods (CDR) which aims to reduce the CO_2 content in the atmosphere. Using climate engineering may lead to a delay in reducing CO2 emissions and as a result, geoengineering could be required for centuries to counteract CO_2 warming (*MacMartin et al.*, 2014). Most of the proposed SRM climate engineering schemes carried out in the atmosphere or space are based on increasing planetary albedo. Solar Radiation Management schemes offer relatively low-energy costs and short lead times for technical implementation and would act rapidly to reduce temperature anomalies caused by greenhouse gas emissions (*Zhang et al.*, 2015), with significant decrease occurring within 1 to 2 years (*Bala*, 2009). In this paper, we will focus on the solar radiation management methodology.

Solar geoengineering (alternatively, SRM, or solar radiation modification or solar climate engineering) is a set of proposed technologies intentionally alter the Earth's radiative balance by offsetting the global warming effect of greenhouse gases by reflecting incoming solar radiation (sunlight) back into space to avoid warming other than changing atmospheric concentrations of greenhouse gases (*Council*, 2015; *Irvine et al.*, 2016). The offset or compensate the greenhouse gas induced warming only requires the reduction of small fraction of incoming sunlight to the Earth. Solar geoengineering has been receiving increased attention in recent years as a potential temporary solution to offset global warming (*Kravitz et al.*, 2021). Six proposed solar geoengineering approaches to reflect more sunlight to reduce global warming are shown in Figure 1.1, including giant space mirrors, stratosphere aerosols injection, marine clouds brightening, making the ocean surface more reflective, growing more reflective plants, and whitening roofs and other built structures. In this study, we will primarily evaluate the effect of the giant space mirrors, which reflects incoming solar radiation into the outer space.

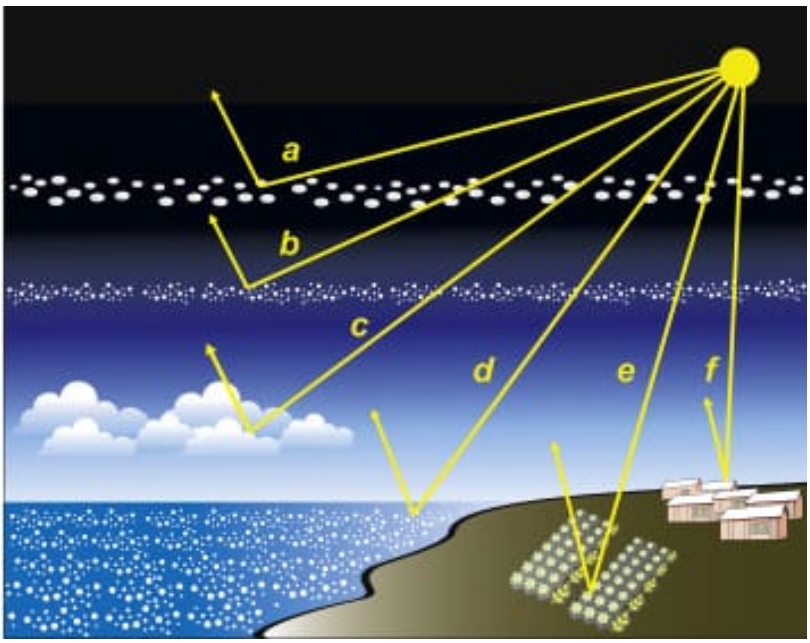

Figure 1.1: Schematic diagram illustrating solar geoengineering approaches, a- Giant space mirrors, b- Stratosphere Aerosols injection, c- Marine clouds brightening, d- making the ocean surface more reflective, e- Growing more reflective plants, and f- Whitening roofs and other built structures (*Caldeira et al.*, 2013)

Numerical climate model simulations have consistently indicated that solar radiation management could not only reduce the Earth's temperature but also affect the precipitation pattern at global and regional scales. Many idealized climate model simulations have been performed in which the solar radiation is uniformly reduced by a certain amount to offset the warming caused by increased atmospheric CO_2 e.g. (*Govindasamy and Caldeira*, 2000; *Govindasamy et al.*, 2003; *Bala et al.*, 2008; *Caldeira and Wood*, 2008; *Irvine et al.*, 2016; *Kravitz et al.*, 2013). Solar geoengineering could quickly reduce global mean temperatures at relatively low cost (*McClellan et al.*, 2012). Although SRM schemes can act rapidly to mitigate climate change with significant global mean temperature decreases as evidenced by models, unwanted side-effects, such as diminished rainfall in some regions would certainly also occur alongside the intended effects (*Zhang et al.*, 2015).

Several simulation studies have been performed using the solar geoengineering schemes where incoming solar radiation was reduced to compensate the atmo-

spheric carbon dioxide (CO_2) induced warming. *Ban-Weiss and Caldeira* (2010); *MacMartin et al.* (2014) determined an optimal reduction in solar radiation in both the top of the atmosphere and time therefore the geoengineered climate is more similar to the control climate. *Govindasamy and Caldeira* (2000) showed that solar geoengineering with globally uniform 1.8% reduction in incoming solar radiation would largely compensates global and annual mean surface temperature change for a doubling of atmospheric CO_2 content from pre-industrial levels. The solar experiment cools the climate by nearly identical amount of the warming caused by the doubled CO_2 (*Govindasamy et al.*, 2002). Furthermore, *Govindasamy et al.* (2003) in their latter study showed that global uniform 3.6% reduction in solar radiation mitigate the climate impact of quadrupling of atmospheric CO_2 and cools the Earth from its 4xCO_2 state. They further showed that such a reduction in incoming solar radiation would also largely compensate the regional or seasonal climate change. To offset the warming by the doubled atmospheric concentration of CO_2 globally, *Caldeira and Wood* (2008) suggested that a uniform 1.84% reduction in incoming solar radiation at the top of the atmosphere could noticeably reduce regional and seasonal climate change from increased atmospheric carbon dioxide (CO_2) . In a recent study (*Kravitz et al.*, 2013), it was shown that the climate impacts on quadrupling CO_2 from the preindustrial concentrations could be reduce by global uniformly reduction in incoming solar radiation. In their study they further showed that the reduction largely offsets the global mean surface temperature change to prevent the Arctic sea ice loss. However, reduction in insolation might disturb the global hydrological cycle (*Govindasamy et al.*, 2003; *Bala et al.*, 2008; *Caldeira and Wood*, 2008; *Kravitz et al.*, 2013). According to *Russotto and Ackerman* (2018), the required solar constant reduction in solar geoengineering experiments for 4xCO_2 is between 3.2% and 5.0%, depending on the model, and these values are uncorrelated with the model's equilibrium climate sensitivity, while a formula from the experiment specifications based on the model's effective

CO_2 forcing and planetary albedo is well correlated with but consistently under predicts the required amount of solar reduction.

This master thesis seeks to evaluate the feasibility and impacts of geoengineering using SRM scheme. We compare results from three kinds of model simulations: pre-industrial (PI-Control), post-industrial enhanced warming (abrupt4×CO_2) and solar geoengineering, implemented to compensate the radiative impacts of the abrupt4×CO_2, (thus, quadrupled of the atmospheric CO_2 content). The main objective of this thesis is to compare post-industrial abrupt4×CO_2 warming climate with Pre-industrial climate to assess the impacts of the CO_2 on the climate with no reduction in solar constant to offset the global warming effect of greenhouse gases, and then compares the an idealized solar geoengineering simulation experiment in which the greenhouse gas induced warming in the global mean surface temperature is offset by reduction in the solar constant with the abrupt4×CO_2 warming climate.

This master thesis is written in the following order. In section. 2, the employed climate model, i.e., the AWI-ESM and the experimental design are described. The simulated global warming world and geoengineering climate anomalies in temperature, precipitation and sea ice fractions are presented in Section 3. The section 4 summarizes and concludes this study, and outlines the hypothesis and the future steps during the master thesis project.

Chapter 2

Model and Methods

2.1 AWI Earth System Model (AWI-ESM)

The Alfred Wegener Institute Earth System Model (AWI-ESM) (*Sidorenko et al.*, 2019) is used to perform the simulations of this study. The AWI-ESM was developed by the Alfred Wegener Institute for Polar and Marine Research. It consists of the atmospheric model ECHAM6 and the Finite Element Sea ice-Ocean Model (FESOM), version 1.4. The simulations conducted in this study used the AWI-ESM with atmosphere resolution of 1.875×1.875 degree (approximately 200 km near equator). Ocean and sea ice were simulated on a mesh with resolution varying from nominal one degree in the interior of the ocean to 1/3 degree in the equatorial belt and ∼24 km north of 50°N. AWI-ESM has previous widely applied in the simulations of paleo, present and future climates (*Lohmann et al.*, 2020; *Shi et al.*, 2020; *Kageyama et al.*, 2020; *Brierley et al.*, 2020; *Yang et al.*, 2020a)

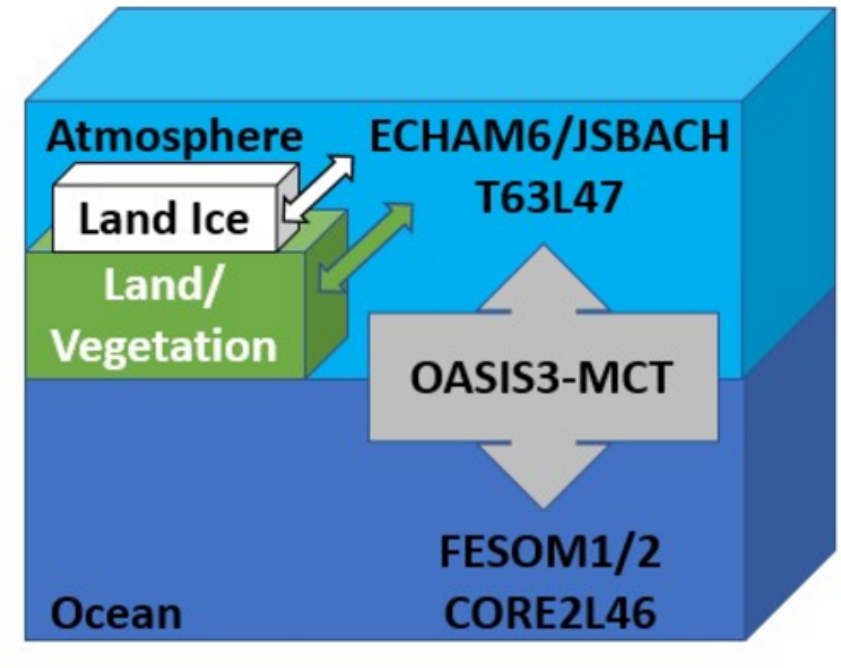

Figure 2.1: ECHAM6 computes 12 air-sea fluxes based on 4 surface fields provided by FESOM1/2. The 1 hourly averaged fields and 1 hourly accumulated fluxes are mapped between the model components every 1 hour using the OASIS3-MCT coupler (https://fesom.de/models/awi-esm/).

2.2 Experimental Design

We perform three set of simulations. Firstly, a pre-industrial control simulation is carried out under the pre-industrial CO_2 (i.e. 284 ppmv) forcing and normal amount of incoming solar flux (sunshine) of 1360.744 Wm^{-2}. It is denoted PI-Control. This experiment is integrated for 600 years. The last 100 years results are used to represent the climate condition without anthropogenic global warming. To obtain the pattern of anthropogenic climate change, we run another experiment, namely, the abrupt4×CO_2 experiment, in which the atmospheric CO_2 concentration is instantaneously quadrupled from the PI-Control level with normal amount of incoming solar flux. This experiment is initialised from 600th model year of the pre-industrial control experiment. To evaluate the impact of geoengineering on climate change, we set up another two experiments, which apply uniformed reduction of the incoming solar radiation at TOA globally and regionally over the poles (higher than 60 degrees), respectively. In the two geoengineering simulations, the greenhouse gases forcing is kept identical to the abrupt4×CO_2 experiment. The abrupt4×CO_2 simulation and all the geoengineering simulations were run for 200 elapsed model years with the first 100 years being discarded and the last 100 years being used to compute climate statistics.

To know the amount of insolation required to compensate 4×CO_2 at TOA, we perform sensitivity analysis and calculate the equilibrium climate sensitivity and the effective radiative forcing. The equilibrium climate sensitivity, is the long-term temperature rise (equilibrium global mean near-surface air temperature) that is expected as result from a doubling of the atmospheric CO_2 concentration. The effective radiative forcing is the instantaneous radiative imbalance caused by increasing greenhouse gases. To restored radiative equilibrium, the climate system response to a radiative forcing with a change in net downward radiative imbalance (TOA) which is proportional to global-mean surface air temperature. We

then reduce the net top shortwave radiation by a factor of the effective radiation forcing.

Theoretically, a 1.8% (3.6%) of solar reduction is effective to offset the radiation imbalance caused by doubling (quadrupling) of CO_2. However, due to the feedback in the climate system, this value varies in different models. Our AWI-ESM sensitivity tests indicate that a glabally 4.2% solar radiation reduction is approximately the amount needed to offset the global mean temperature effect of the quadrupled CO_2 concentration in the atmosphere.

Besides the glabally uniform 4.2% solar radiation experiment, two more simulations focusing on the polar regions were performed: one with a 4.2% reduction in insolation over of 60 degrees (60^o) over both Northern and Southern Hemispheres and the other with quadrupled of the global reduction that is 16.8% reduction in the insolation over 60^o. In practice, this reduction in incoming solar radiation at the top of the atmosphere on the Earth could be affected through the placement of artificial solar eclipse or solar-shields in space between the Earth and Sun to reflect the solar radiation.

Simulation	CO_2 (ppm)	Region of insolation reduction	Insolation reduction (%)
PI-Control	284	-	-
Abrupt4×CO_2	1136	-	-
Global_4.2	1136	global	4.2
Polar_4.2	1136	60^o N - 90^o N and 60^o S - 90^o S	4.2
Polar_16.8	1136	60^o N - 90^o N and 60^o S - 90^o S	16.8

Table 2.1: Simulations include pre-industrial control and 4×CO_2 climate that differ in atmospheric CO_2 content and the simulations in which solar insolation is reduced at various levels globally, or regionally at the latitudes higher than 60 degrees over both hemispheres.

Chapter 3

Results

In this section, the results from the three sets of simulations are presented and the anomalies of the surface air temperature, precipitation and sea ice fraction in the Northern Hemisphere and Southern Hemisphere are discussed. The climate engineered simulation results which is implemented to compensate the radiative impact of $4\times CO_2$ are compared to the quadrupled CO_2 (abrupt$4\times CO_2$) and PI-Control simulations.

3.1 Climate change under GHG forcing

3.1.1 Climate Sensitivity

Climate Sensitivity refers to global temperature rise that occur in response to a doubling of CO_2 concentration in the atmosphere compared to pre-industrial levels and is determined by some radiative feedback mechanisms associated with temperature, water vapor, cloud, and surface albedo change (*Block and Mauritsen*, 2013). Estimation of the equilibrium climate sensitivity was performed on the abrupt$4\times CO_2$. According to *Meehl et al.* (2020), the multi model mean ECS from the Gregory method, calculated over the full 150-year period of the abrupt$4\times CO_2$ experiment, is 3.7°C. The range of equilibrium climate sensitivity is from 1.8°C

to 5.6°C for the current generation of earth system models participating in the Coupled Model Intercomparison Project Phase (CMIP6).

In the abrupt4×CO_2 simulation, CO_2 has increased from its pre-industrial level of 284 parts per million (ppm) to around 1136 ppm, as shown in Table 2.1. The equilibrium temperature was obtained by extrapolating a linear fit of the data points (that is, the individual years) when the model reached its new equilibrium to a zero TOA energy balance. The global mean surface air temperature was found to be increased by 6.7 K. The effective radiative forcing for the abruptly quadrupled CO_2 concentration was estimated by finding the intercept of the linear fit with the ordinate (TOA radiative imbalance) using the Gregory's method (*Gregory et al.*, 2004), and was found to be about 7.0 Wm^{-2} at the TOA. To obtain the equilibrium climate sensitivity and effective radiative forcing for a doubling of the CO_2 concentration, the equilibrium temperature and effective radiative forcing in the 4×CO_2 simulation are divided by 2. So, in AWI-ESM, the equilibrium climate sensitivity and effective radiative forcing are found to be 3.35 K and 3.5 Wm^{-2} respectively. The climate sensitivity analysis is shown in Figure 3.1.

The global mean surface air temperature increased in the abrupt4×CO_2 simulation as a results of the radiative imbalance in radiation at the top of the atmosphere caused by the abruptly quadrupled CO_2 concentration in the atmosphere. The radiation imbalance found in this study is within the range of radiative imbalance found by (*Kravitz et al.*, 2013), which the effective radiative forcing for 4×(CO_2) forcing is about 6 to 9 Wm^{-2}.

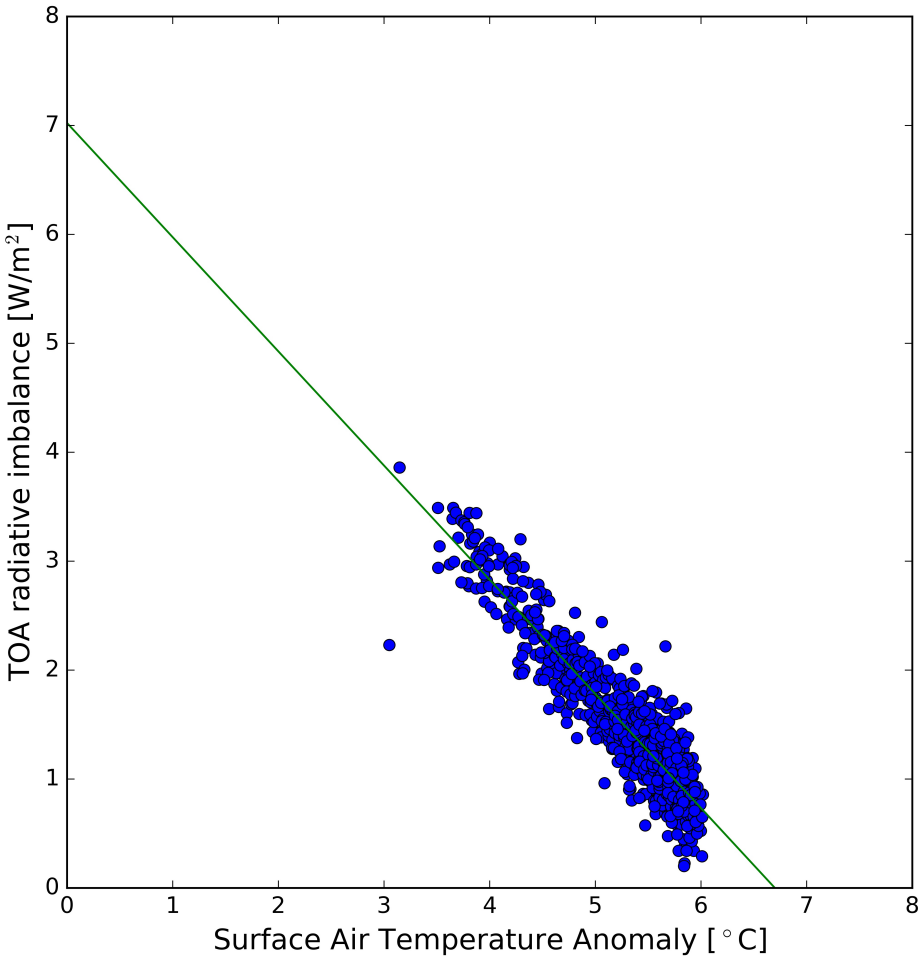

Figure 3.1: The anomalies are calculated as difference between the abrupt4×CO_2 and PI-Control run. Equilibrium climate sensitivity on the 4×CO_2 relative to the PI-control. The blue dots represent individual year of surface temperature anomaly and radiation imbalance at the TOA. The green line is the linear regression of the individual years. The effective radiative forcing is the radiation imbalance when global mean temperature has no change. The equilibrium climate sensitivity is the final global mean temperature anomaly when the outgoing long wave radiation is balanced by the incoming solar radiation.

3.1.2 Surface Air Temperature

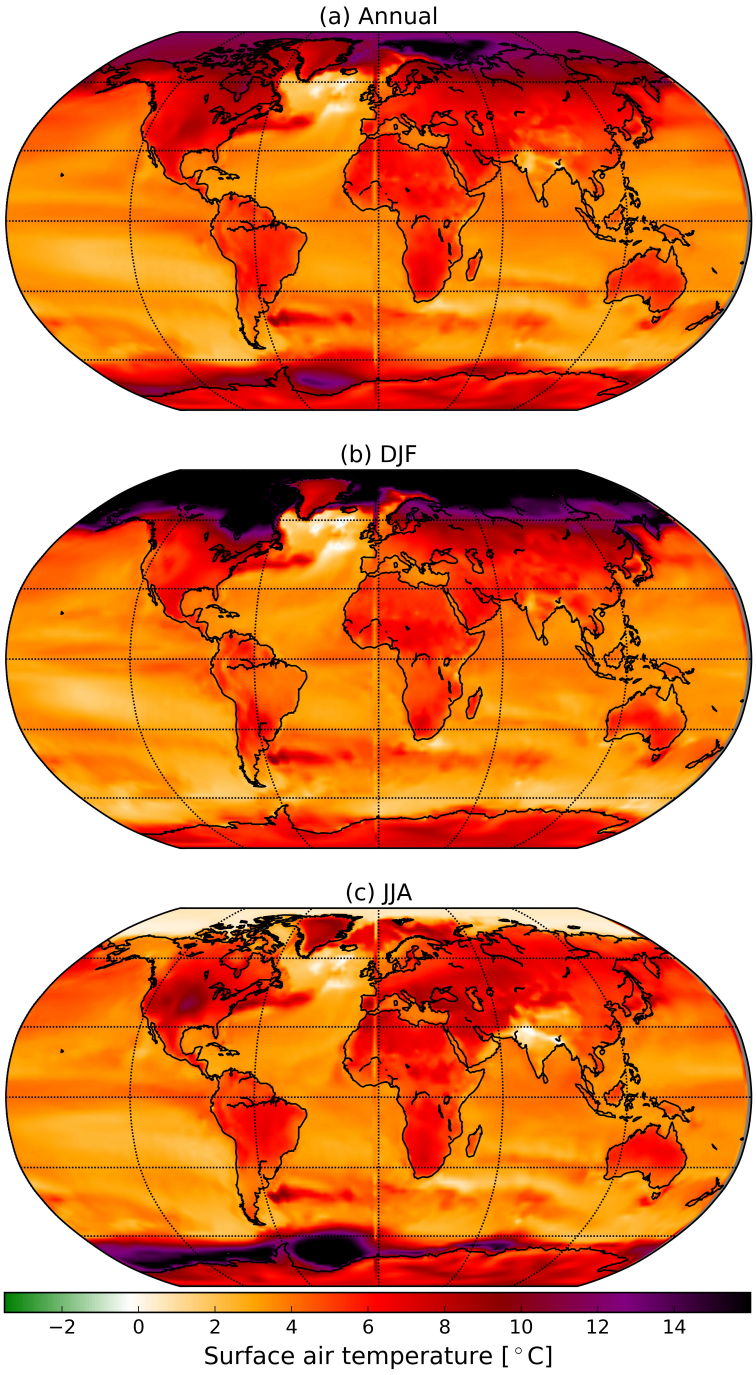

Figure 3.2: Global surface air temperature anomalies for (a) Annual, (b) December-January-February (DJF) and (c) June-July-August (JJA) average relative to the PI-Control simulation in the quadrupled $4\times CO_2$ simulation.

Figure 3.2 shows the surface air temperature anomalies in the quadrupled CO_2 (abrupt $4\times CO_2$) simulation. In general, the warming in the abrupt$4\times CO_2$ is observed in all regions in both annual and seasonal surface air temperatures. The abrupt$4\times CO_2$ simulation shows a global mean surface air temperature rise of 4.7°C (Table 3.1) after 200 years. The annual mean temperature anomalies show strongest positive anomalies in the high latitudes. Moreover, the temperature raises over the land are higher than that of the ocean (Figure 3.2a). The surface air temperature anomalies in the winter (DJF) and summer (JJA) are significantly different. The DJF mean surface temperature at the Northern pole (Arctic region) is found to be significantly greater than the annual mean temperature, whereas the JJA mean surface temperature appears to have been particularly significant in the Southern pole (Antarctica region). At the high latitudes, the quadrupled CO_2 simulation warms more during the winter season. Because the high latitudes have feedback processes involving snow and ice albedo which make their temperature response more sensitive to changes in radiative forcing (*Caldeira and Wood*, 2008). This leads to reduction in amplitude of the seasonal cycle (*Govindasamy and Caldeira*, 2000). Amplified winter warming in the Arctic in the abrupt$4\times CO_2$ simulation could be contributed by the large exchanges of heat and moisture from the ocean to the atmosphere. The rise in mean surface air temperature appears to have risen more over the land than over the ocean and this is because land has smaller heat capacity than water.

At the polar regions, when there is reduction in sea ice content, there is a strong or greater transfer of heat and moisture to the atmosphere, which in combination with ice albedo feedback amplifies the warming at the region. The rapid warming seen at the polar regions, in particular the Arctic can be interpreted by the increased in absorption of sunlight resulting in less reflective surface in the region. This dramatical warming over the polar regions could lead to melting of Greenland ice sheet and Antarctica ice sheet, and would eventually cause sea level rise, as well as

bottom water formation and also affects the patterns of precipitation. The retreat of sea ice in all seasons has already had profound impacts on the energy balance of the Arctic and has contributed to Arctic amplification, i.e. the faster warming in the Arctic compared to mid-latitudes, particularly during autumn and winter (*Walsh*, 2014).

3.1.3 Precipitation

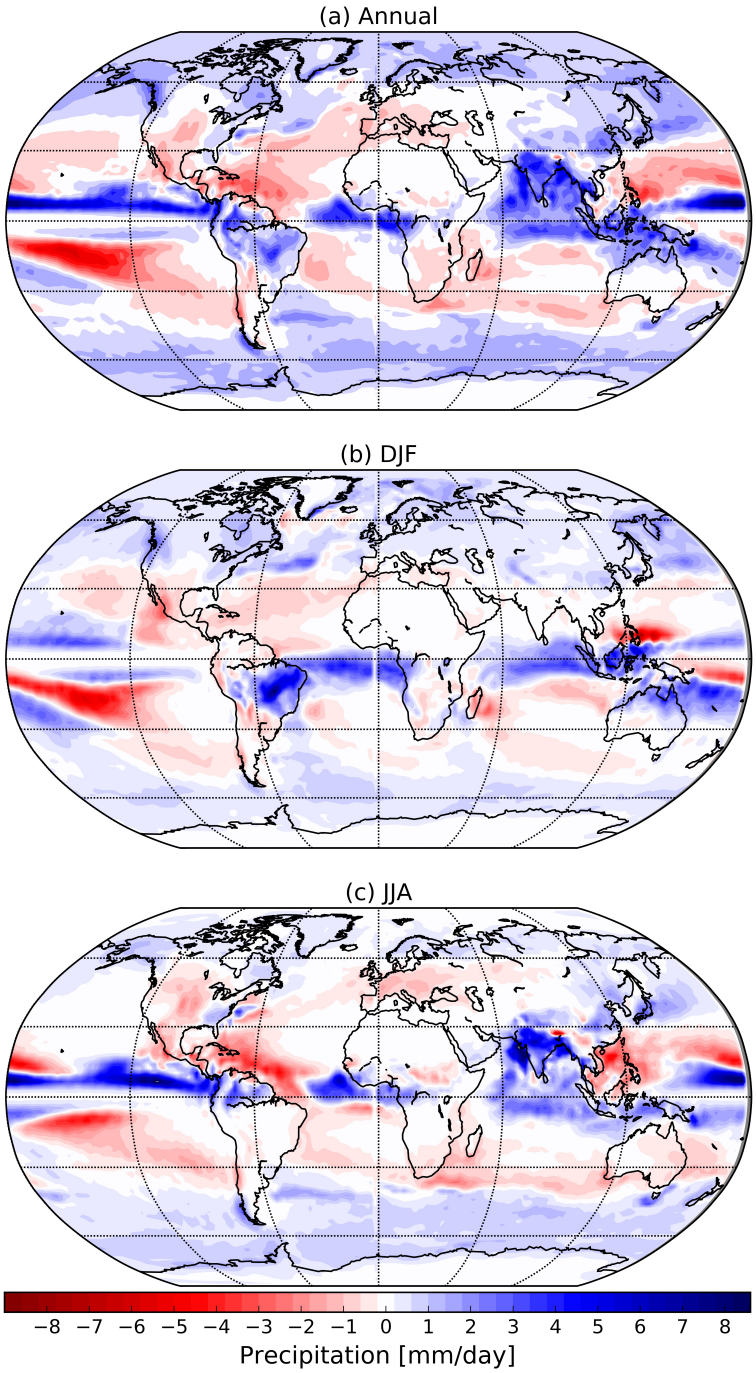

Figure 3.3: Global Precipitation anomalies for (a) Annual, (b) DJF and (c) JJA average relative to the PI-Control simulation in the abrupt4×CO_2 simulation.

The abrupt4×CO_2 simulation shows a significant (7.5±0.62%) increase in global average of mean precipitation, but with a strong spatial inhomogeneous. There

is an increase in both annual and seasonal precipitation at the high latitudes and at equatorial regions. The most increased in annual precipitation occurs in some regions, notably over the equatorial Pacific, Eurasia, Brazil and the central South America–Caribbean Sea. Precipitation increases in the tropics and decreases in the subtropics over ocean in both Northern and Southern Hemispheres. The summer (JJA) precipitation is very similar to annual precipitation change, tropical precipitation increases over the summer (JJA) and slightly decrease over the winter (DJF). This is because the summer hemisphere is dominated by the ascending branch of the Hadley circulation whiles the winter hemisphere is dominated by the ascending branch of the Hadley circulation (*Chou and Lan*, 2012). Precipitation increases over oceans is much larger than that over land. There is more precipitation in the South Pacific Convergence Zone, however, the precipitation significantly decreases in some regions, the decreases are especially evident in the Mediterranean, South Africa, Northern and Western Europe, northern part of North America over California, the southern part of South America, Australia, East Asia, Southeast Asia and the centre of the North Atlantic. The abrupt$4\times CO_2$ simulation shows significant positive anomalies over the Intertropical Convergence zone (ITCZ) and in the high latitudes, but significant negative anomalies in the subtropics and some areas in the tropics. In general, there have been decreases in precipitation in the subtropics and tropics outside of the monsoon trough, and increases in land precipitation at higher latitudes and in the equatorial regions. Such precipitation pattern change is partly driven by the expansion of Hadley Circulation or poleward shift precipitation pattern (*Hu and Fu*, 2007; *Lu et al.*, 2007; *Yang et al.*, 2022), as a result of poleward advancing midlatitude meridional temperature gradients (*Yang et al.*, 2020b). Figure 3.3 shows that the regions with more precipitation, like the central tropics and high latitudes, increase in precipitation whereas the regions with less precipitation, such as the subtropical regions, decrease in precipitation. This means that the annual range of precipita-

tion that has already been large will become even larger under the abrupt4×CO_2 global warming, a phenomenon called dry gets drier, wet gets wetter, as a result of intensified hydrological cycle (*Chou and Lan*, 2012).

3.1.4 Sea Ice

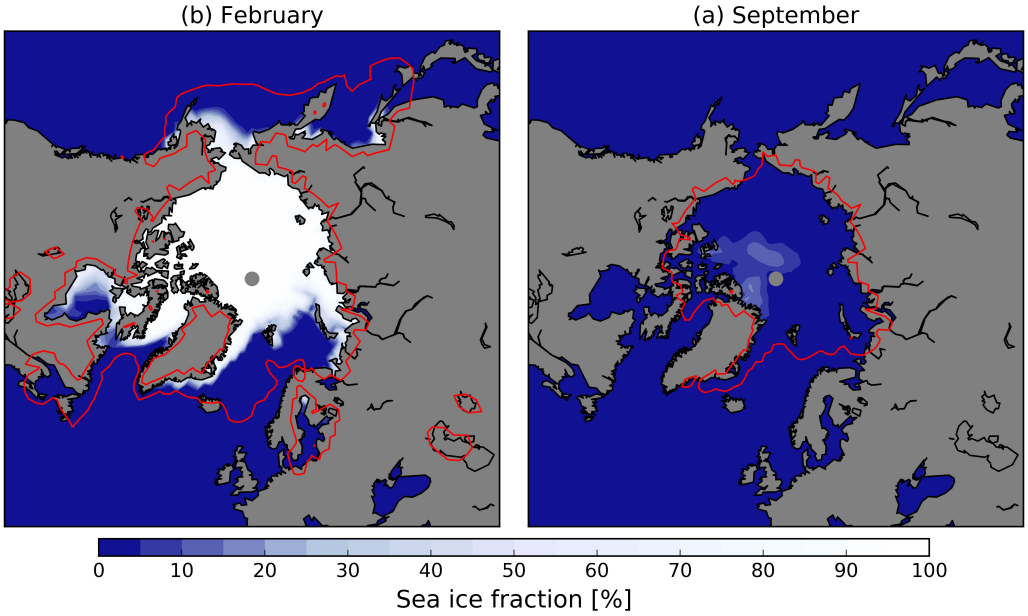

Figure 3.4: (a) February and (b) September Arctic mean sea ice fraction in the abrupt4×CO_2 simulation. The red contour lines represent the PI-Control sea ice edge (5%) for comparison. Higher values are represented in white and lower values in light blue, and ocean is represented by dark blue colour.

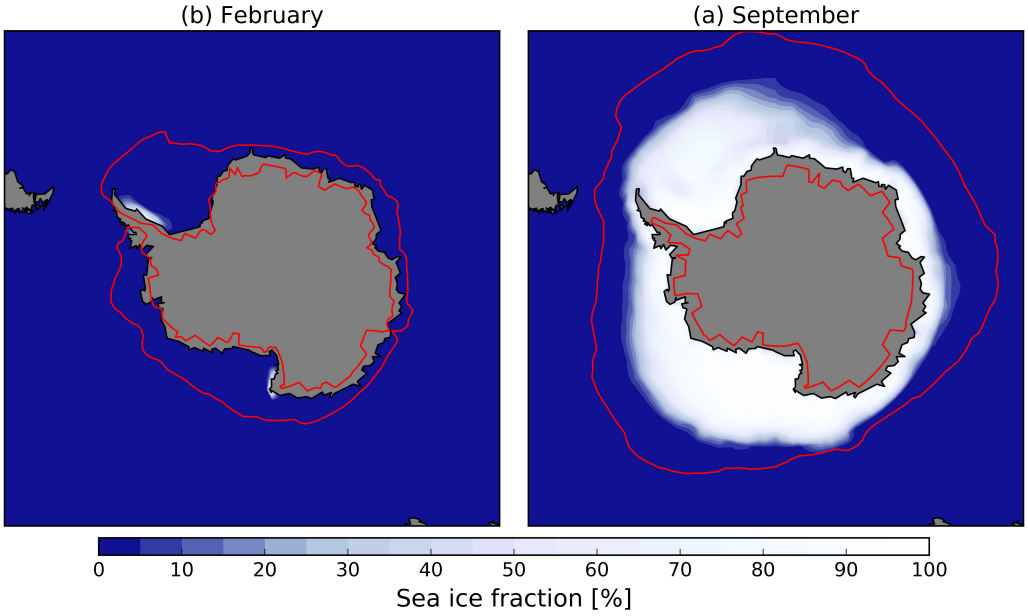

Figure 3.5: (a) February and (b) September Antarctic mean sea ice fraction in the abrupt $4\times CO_2$ simulation. The red contour lines show the PI-Control sea ice edge (5%) for comparison. Higher fraction of sea ice is represented in white and lower values in light blue, and ocean is represented by dark blue colour.

The Arctic ice reaches its maximum extent in March, and minimum extent at the end of the summer thus, in September. During autumn and winter, Arctic sea ice regrows as less or no sunlight reaches the Arctic and air temperatures begin to drop in the region. The total area covered by ice increases through the winter, usually reaching its maximum extent at the end of February or in early March. Figure 3.4 shows the sea ice extent in both of these months. Reduction in Arctic sea ice is one of the most visible signs of climate change on Earth. Sea ice plays an important role in the Earth's climate by regulating the exchanges of heat and moisture between the atmosphere and the polar ocean. When sea ice melts, the surface albedo is lowered, and the amount of incoming solar radiation absorbed by the ocean surface increases, which further enhances ice melt (*Stroeve and Notz*, 2018), generating positive feedback for increasing the surface temperature.

From the abrupt$4\times CO_2$ simulation, the Arctic and Antarctic sea ice is virtually absent during the late summer and there is essentially ice-free summer at some

point as shown in Figure 3.4b because of the more amplified warming in the polar regions (Figure 3.2). The abrupt4×CO_2 simulation does not show much reduction in February sea ice extent (Figure 3.4a) as compared with the PI-Control sea ice extent. The Arctic and the Antarctic annual mean sea ice fraction in the the abrupt4×CO_2 simulation is reduced by 56% and 65.0% relative to the PI-Control, respectively. The sea ice coverage over the Arctic Ocean decreased substantially in September with only a little ice found around the central and western Arctic near Canadian Archipelago. The reduction in Arctic sea ice is particularly pronounced in the East Siberian, Canadian Archipelago, Chukchi, Beaufort Seas and around the Greenland. The sea ice extent appears to be regrown during the following winter (February mean) with a little reduction over the Eurasian side of the Arctic Ocean and the subpolar of Northern Ocean. With this climate, Arctic will lose much of its protective ability to reflect incoming sunlight back to the space from the Earth without summer sea ice and this will eventually cause Arctic amplification. The reduction in Antarctic summer (February) sea ice is pronounced all over the Southern Ocean, with little ice left over the Antarctic Peninsula on the Weddell sea. The most reduction in September ice occurs in the Eastern Antarctic over the Indian ocean sector. The reductions observed in sea ice thickness and coverage are impacting the Earth's energy balance already. The seasonality in heat exchange between the upper ocean and the atmosphere is expected to be stronger with a seasonally ice-free Arctic (*Tietsche et al.*, 2011).

3.2 Global Uniform Solar Radiation Management

3.2.1 Surface Air Temperature

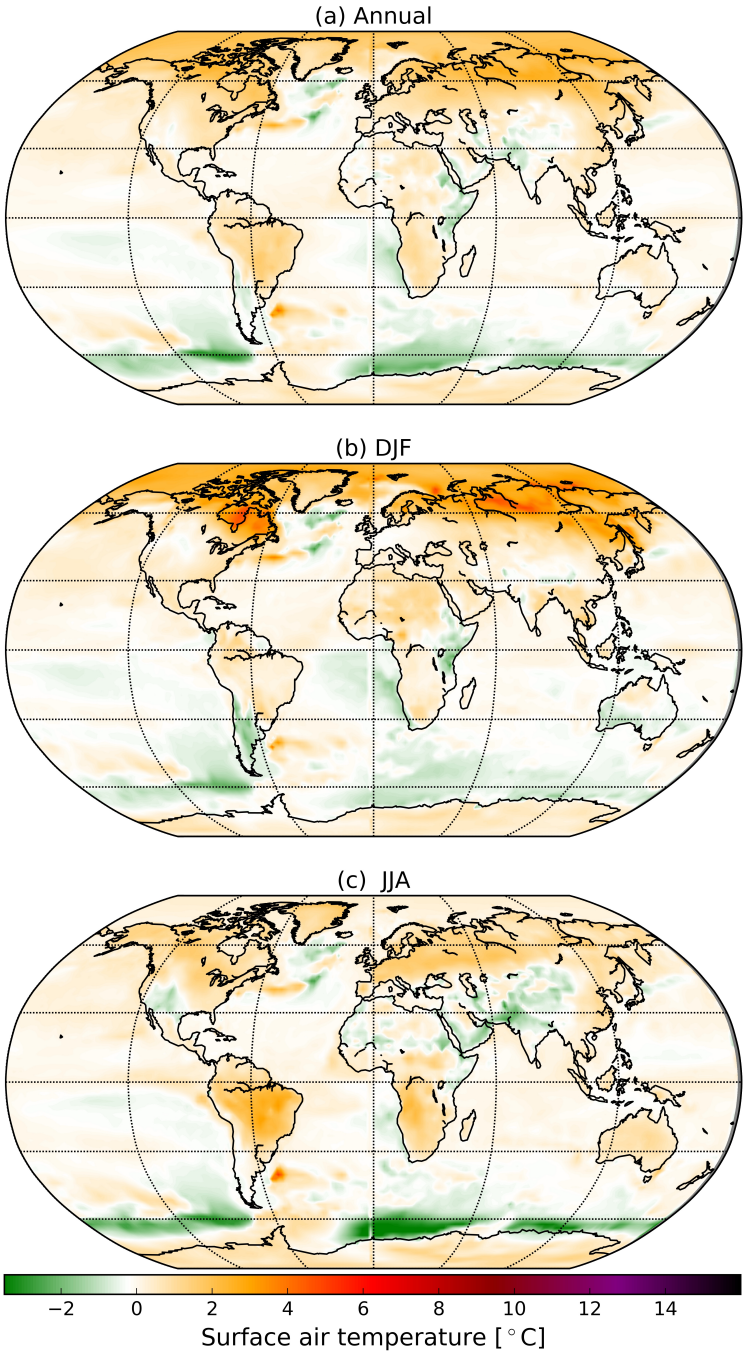

Figure 3.6: Global surface air temperature anomalies for (a) Annual, (b) December-January-February (DJF) and (c) June-July-August (JJA) average relative to the PI-Control simulation in the Global_4.2 climate engineered simulation.

Earlier study by *Govindasamy et al.* (2003), suggested that 3.6% reduction in solar radiation could offset the induced warming caused by $4\times CO_2$. Most previous studies, such as *Arora et al.* (2011); *Gent et al.* (2011); *Ji et al.* (2014); *Lurton et al.* (2020); *Kelley et al.* (2020), have also noticed different percentages in reduction depending upon the model. We have tried with different magnitude of solar reduction using AWI-ESM, and found 4.2% is a moderate reduction in solar radiation in order to compensate the warming induced by $4\times CO_2$. As shown in Figure 3.6, the climate engineered simulation with uniform Global_4.2 % reduction in incoming solar radiation largely compensates the global annual mean warming from the quadrupling atmospheric CO_2 warming (Figure 3.2). The global uniform 4.2% solar engineering shows a global mean surface air temperature drop of 4.5°C from the abrupt$4\times CO_2$ simulation and slightly rise of 0.2°C over the PI-Control temperature (Table 3.1). It reduced both the global-mean temperature and surface temperatures everywhere compared to the temperatures in the abrupt$4\times CO_2$ simulation. However, reduce solar radiation causes spatial and seasonal temperature anomaly patterns as the warming due to increased CO_2 is due to different spatial distribution of radiative forcing (*MacMartin et al.*, 2018).

The surface air temperature in the engineered world is similar to the PI-Control climate with a minor spatial temperature anomalies. More specifically, there is a significant decrease in surface air temperature in the tropics and subtropics, mostly over the oceans but the residual warming with magnitude of about 3.5 ^{o}C at the polar regions and high latitudes. This is because the climatology maximum averaged solar radiation locates at the lower latitudes. Global_4.2 solar engineering produces strongest net solar reduction over the low latitudes. Comparably, the residual warming over the high latitudes are primarily found in winter season, because high latitude regions have little sunshine during winter. Accordingly, 4.2% solar reduction is not able to completely remove the CO_2 warming in the poles. Besides the general latitude distribution of temperature anomaly, we find that

there is overcooling over the typical upwelling regions, such as the Southern Ocean, the eastern basin of the Southern Pacific Ocean and Southern Atlantic Ocean, and the Northern Atlantic subpolar ocean. It is interesting to note that the reduction in incoming solar radiation decreases more insolation in the summertime (JJA) than the wintertime (DJF), however, there is more reduction in average winter temperature than the summer.

The results of surface temperatures for all seasons show that climate engineering where insolation is reduced may largely compensate the impact of atmospheric CO_2 increased irrespective of the difference in the latitudinal and seasonal pattern of the radiative forcing (*Govindasamy et al.*, 2003).

3.2.2 Precipitation

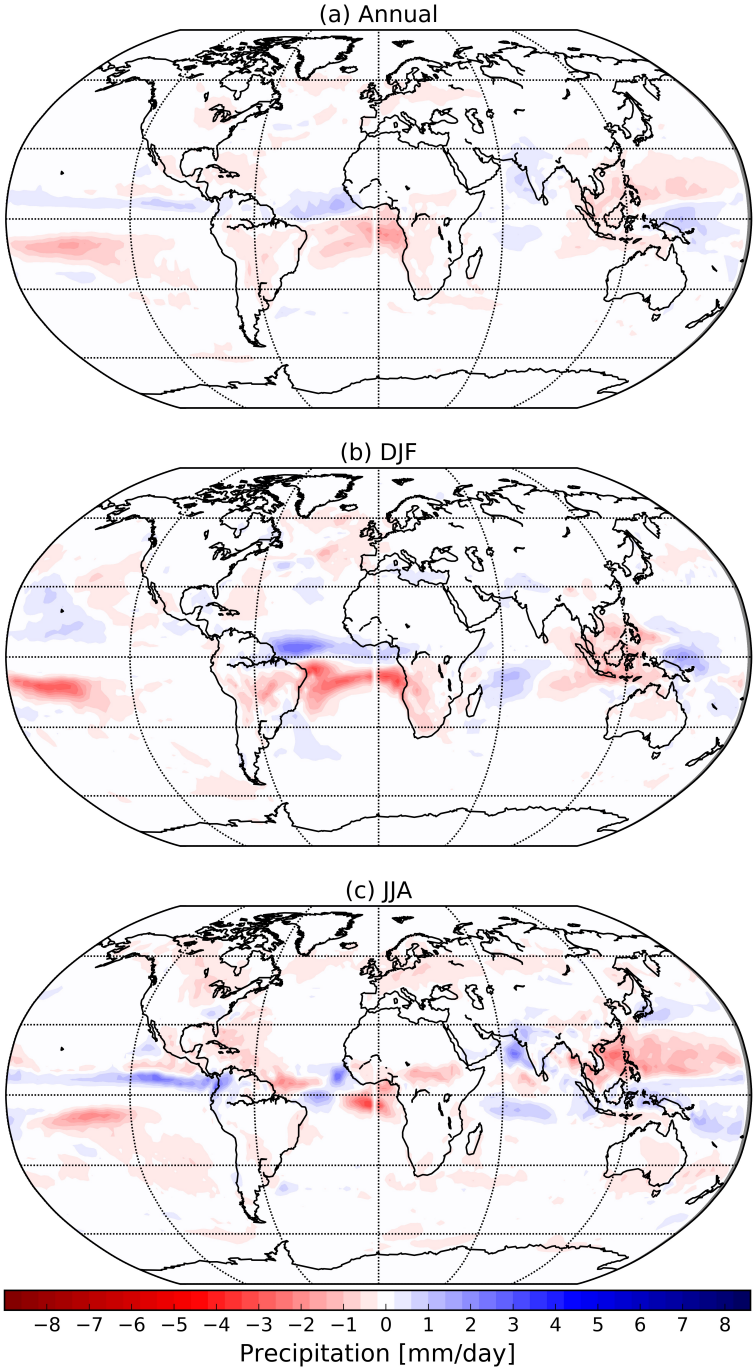

Figure 3.7: Global precipitation anomalies for (a) Annual, (b) December-January-February (DJF) and (c) June-July-August (JJA) average relative to the PI-Control simulation in Global Uniform_4.2% climate engineered simulation.

Reduction in solar radiation cause an overall reduction in global hydrological cycle and hence precipitation of about 2.8±0.47% compared to the global precipitation in the PI-Control simulation. This is likely a result of overall less evaporation due to less incoming solar radiation. Compare to the abrupt4×CO_2 experiment (Figure 3.3 and 3.7), the uniform 4.2% reduction in the incoming solar radiation cancelled out most of the changes in global mean precipitation caused by increasing CO_2. Precipitation patterns under global uniform solar geoengineering decrease over both land and ocean, with similar latitudinal structure. The strongest reduction occurs in the tropics and northern mid-latitudes.

Reduction in solar radiation is not able to restore the PI-Control precipitation pattern. We observe an annual mean northward shift of the Intertropical Convergence Zone (ITCZ), characterising with more/less precipitation over the northern/southern equatorial Atlantic Ocean and eastern Pacific Ocean. This is likely induced by hemisphere asymmetry of temperature changes. More specifically, the Global_4.2 experiment show more residual warming over the Northern Hemisphere than over the Southern Hemisphere (Figure 3.6a). Seasonally, the ITCZ shift is most prominent in the DJF, when the hemisphere asymmetry of temperature reaches its maximum value (Figure 3.6b).

3.2.3 Sea Ice

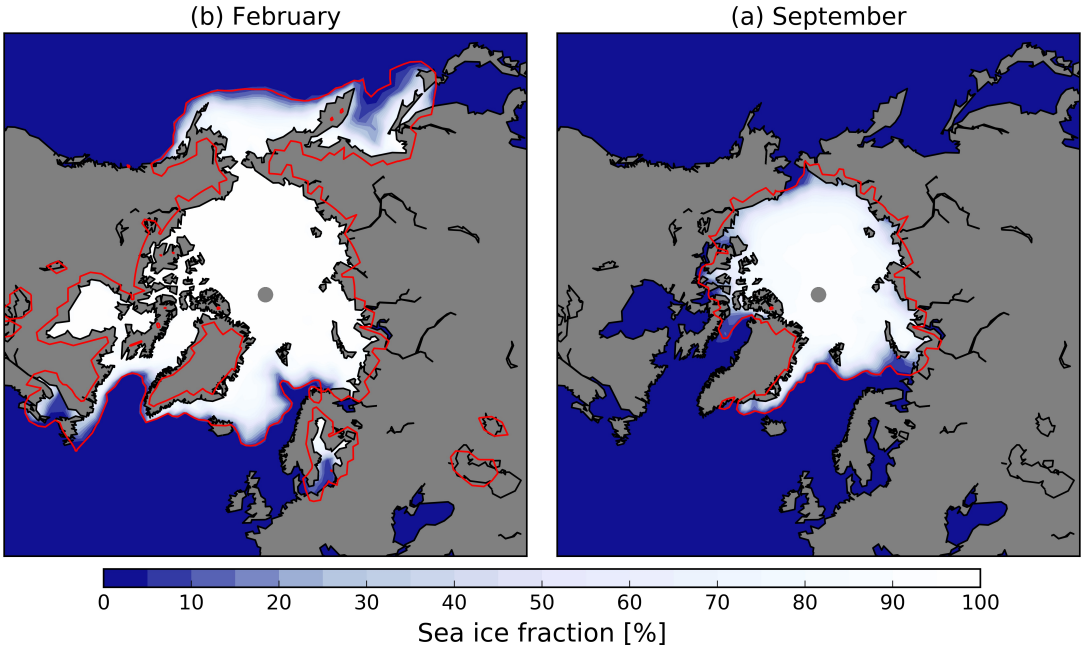

Figure 3.8: Arctic mean sea ice fraction in (a) February (b) September in the Global_4.2 climate engineering simulations. The red contour lines show the PI-Control sea ice edge (5% of sea ice fraction) for comparison. Higher sea ice fraction is represented in white and lower values in light blue, and ocean is represented by dark blue colour.

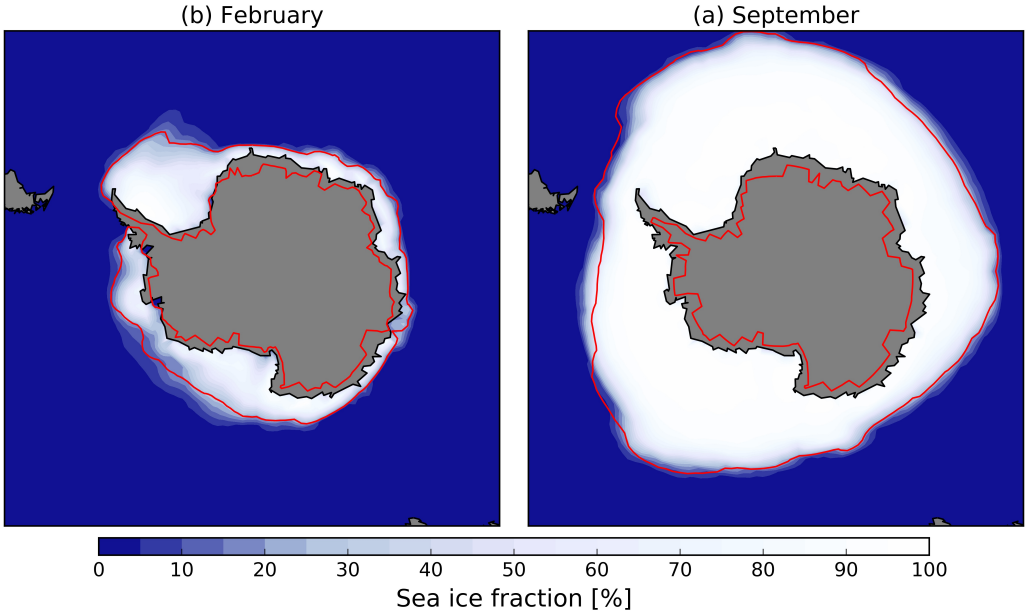

Figure 3.9: Antarctic mean sea ice fraction in (a) February (b) September in the Global_4.2 climate engineering simulations. The red contour lines show the PI-Control sea ice edge (5% of sea ice fraction) for comparison. Higher sea ice fraction is represented in white and lower values in light blue, and ocean is represented by dark blue colour.

The annual average Arctic and Antarctic sea ice fraction is 94.5±2.3% and 110.9±3.8% (Table 3.3) of the PI-Control condition, respectively. The globally uniform 4.2% reduction in solar radiation was able to reflected more sunlight back to space to reduce the global mean surface air temperature and restore the Arctic and Antarctic sea ice. When the surface air temperature stays consistently at or below the freezing point, ice begins to grow in the open ocean. Figure 3.8 shows that, the Arctic sea ice extent in the globally uniform 4.2% simulation is almost restored or recovered in both February and September from its abruptly4×CO_2 state. From Figure 3.8a, the February sea ice extent looks almost similar to the PI-Control sea ice and covers all the coverage areas. The September sea ice that decreased substantially in the abrupt4×CO_2 simulation has almost been recovered in this experiment (Figure 3.8b) as compared to the sea ice extent in the PI-Control simulation. The Antarctic sea ice extent is fully recovered in both February and

September mean (Figure 3.9) with about 10.9% increment over the preindustrial level. The summer sea ice cover regulates the uptake of heat by the Arctic Ocean by reflecting the Sun's rays.

3.3 Polar Solar Radiation Management

3.3.1 Surface Air Temperature

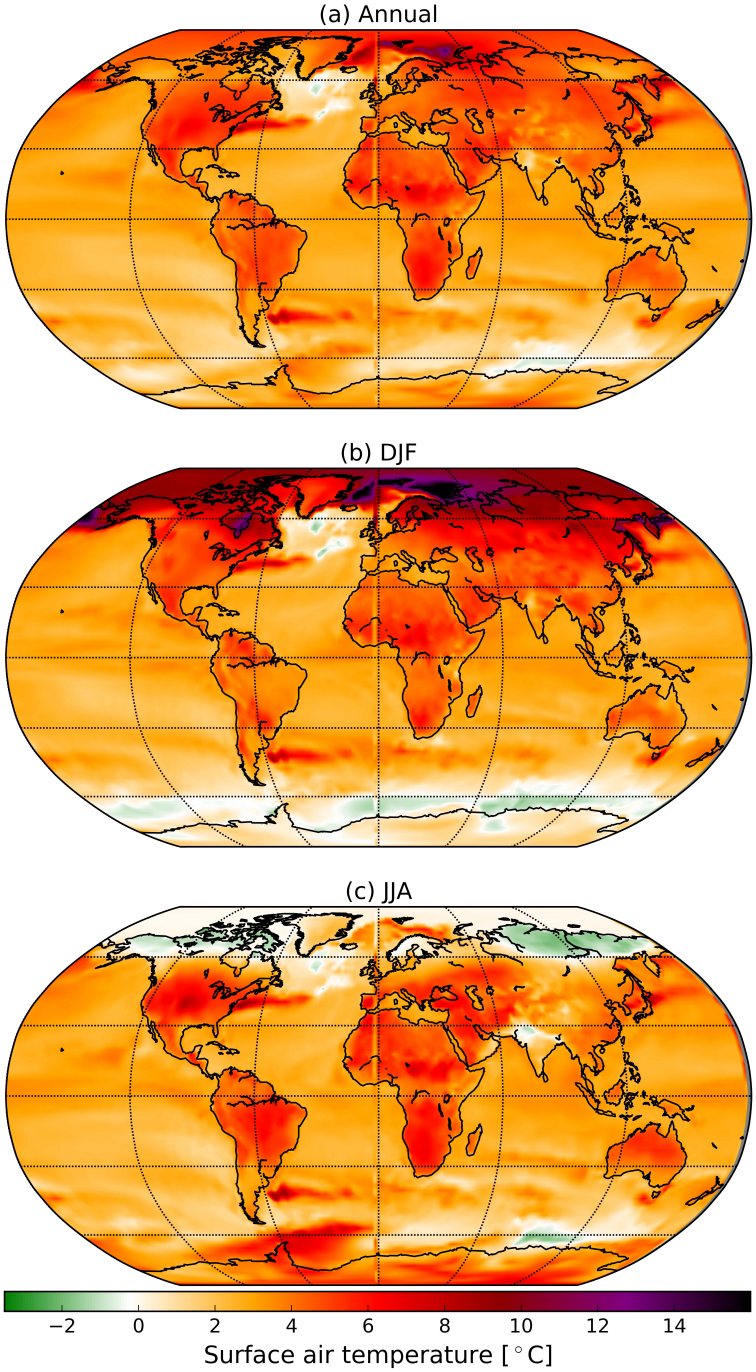

Figure 3.10: Global surface air temperature anomalies for (a) Annual, (b) December-January-February (DJF) and (c) June-July-August (JJA) average relative to PI-Control simulation in the Polar_16.8 climate engineered simulation.

Global uniform solar reduction (sun shading) may economically difficult to achieve. This inspires us to design alternative strategy to just reduce the solar radiation regionally over some important area. Global warming induce dramatic warming over the polar regions, which is potential to cause irreversible disintegration of the Greenland and Antarctic Ice sheets, which are critical for future sea level change. Polar sea ice melt amplifies the warming through positive ice-albedo feedback. Therefore, reduce solar radiation over polar regions may come out to be more efficient in preventing the anthropogenic warming. Polar region has little population, and in the summertime, it has 24 hours sunlight. Considering all these facts, we desire another experiment to compensate the warming just by reducing the incoming sunlight over the polar region, (higher than 60 degrees at both Northern and Southern Hemispheres). We have tested two different reduction amplitudes, i.e. 4.2% and 16.8%. Despite that globally uniform 4.2% solar reduction is able to reduce most of the GHG warming over the polar regions, polar 4.2% solar reduction has little impact on the polar regions.

The Polar 4.2% and 16.8% solar engineering drop the global mean surface air temperature from the abrupt $4\times CO_2$ simulation by 0.4°C and 1.5°C respectively (Table 3.1). The Polar simulation with 16.8% reduction in insolation compensated most of the warming caused by the quadrupling $4\times CO_2$ concentration (Figure 3.2c) in the Hemisphere summer, as shown in Figure 5.1. This could largely prevent the melt of Greenland Ice Sheets and probably also the Antarctic Ice Sheet.

Even though, there are still strong anomalies in surface air temperature during the winter (DJF) as shown in Figure 5.1b, but we mostly care about preventing the summer temperature raise. Moreover, the warming in winter could be beneficial to the people living in the region. The 16.8% reduction in the Polar region also reduce warming globally as compared to the warming in abrupt$4\times CO_2$ simulation as shown in Figure 3.2 , despite the fact the reduction in incoming solar radiation

was done at only the Polar regions over the 60^o North and 60^o South.

3.3.2 Precipitation

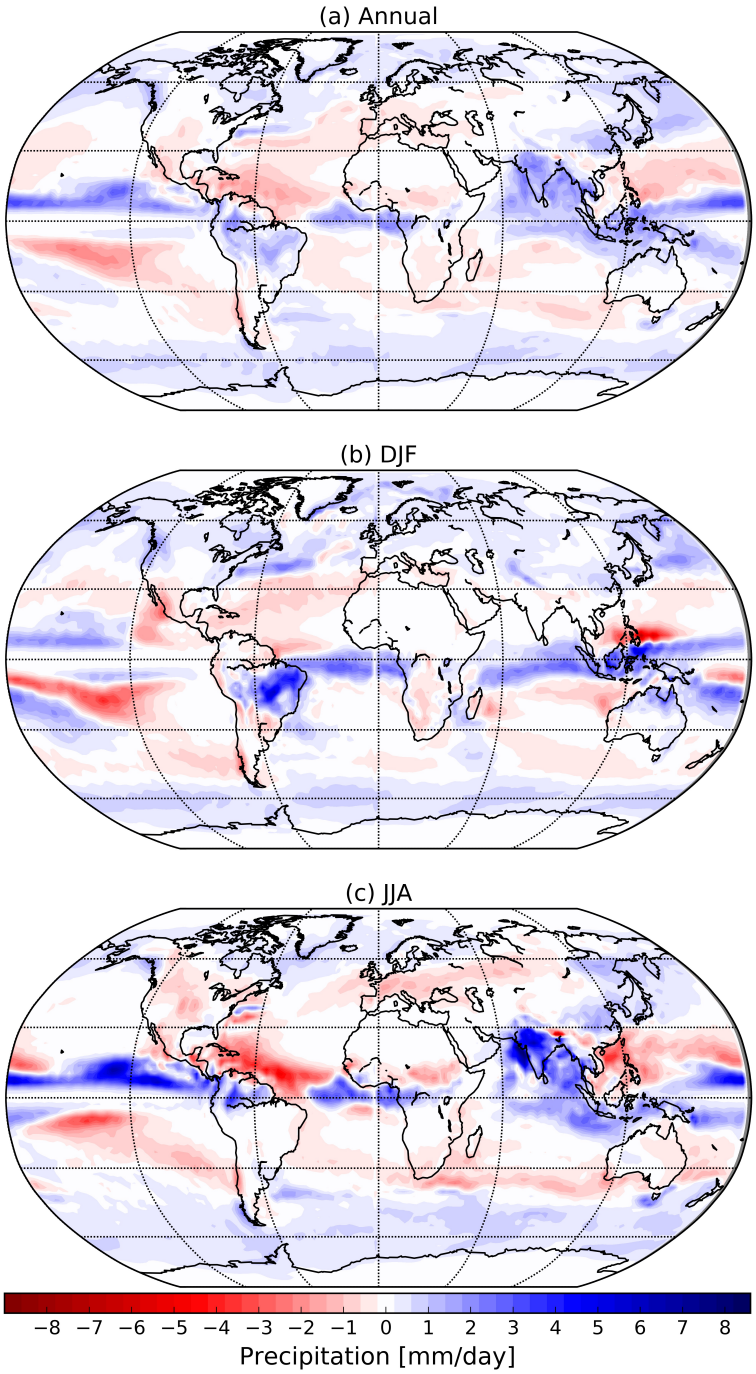

Figure 3.11: Global precipitation anomalies for (a) Annual, (b) December-January-February (DJF) and (c) June-July-August (JJA) average relative to the PI-Control simulation in Polar_16.8 experiment climate engineered simulation.

Solar reduction in polar regions reduce the significant increased in global mean precipitation changes seen in abrupt4×CO_2 to 5.0±0.60% compared to the global precipitation in the PI-Control simulation. Polar_16.8 decreases global precipitation in annual and seasonal mean, with less precipitation over land than the ocean. The changes in precipitation are driven both by the reduction in solar radiation and the increase of atmospheric CO_2 (*Bal et al.*, 2019). However, the results indicate less drop in global mean precipitation compared to the state of precipitation reduction in the Global 4.2 simulation. This is because the reduction was done in the polar regions only and it global effect on abrupt4×CO_2 was not much despite the reduction been more than the amount of solar reduction in the uniform globally 4.2%. The Polar solar reduction has less impact on the seasonal mean precipitation (Figure 3.11) as compared to the state of precipitation in Global 4.2. We find a significant surface decrease of precipitation over most parts of the globe in the annual mean in the Polar 16.8 simulation with most decrease in the tropics. The decrease in precipitation occurs in the tropics because the reduction in solar forcing is strongly experienced there in the annual mean. Although, there are still strong positive and negative precipitation anomalies in Polar 16.8 simulation in reference to the PI-Control.

3.3.3 Sea Ice

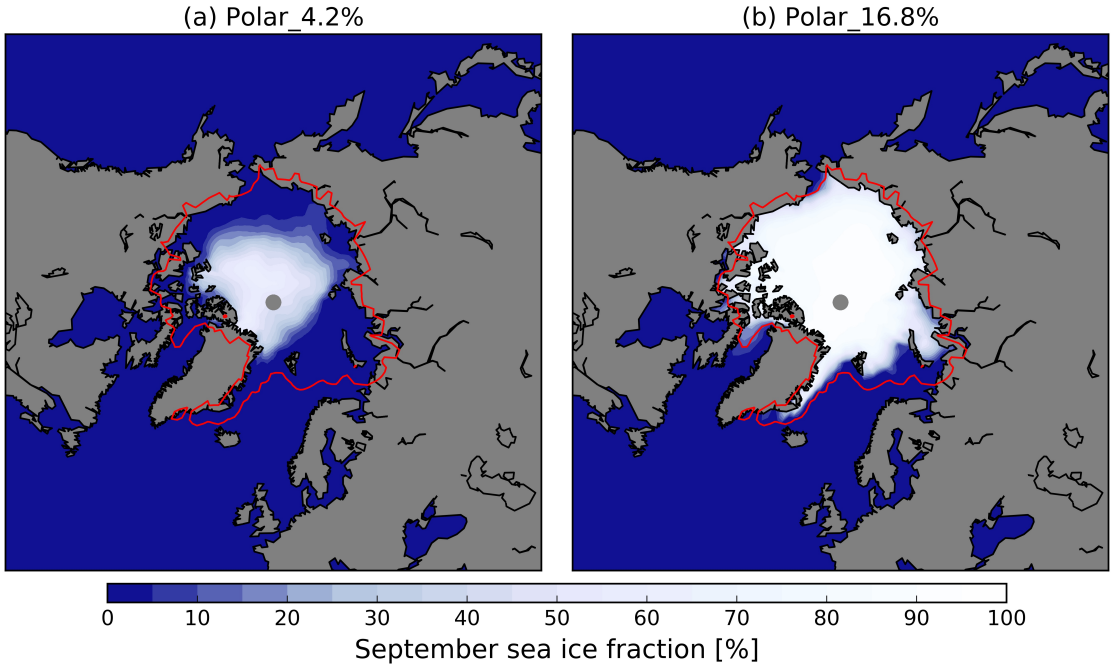

Figure 3.12: Arctic September mean sea ice fraction in the (a) Polar_4.2% and (b) Polar_16.8% climate engineered simulations. The red contour lines show the PI-Control sea ice edge (5% sea ice fraction) for comparison. Higher sea ice coverages are represented in white and lower values in light blue, and ocean is represented by dark blue colour.

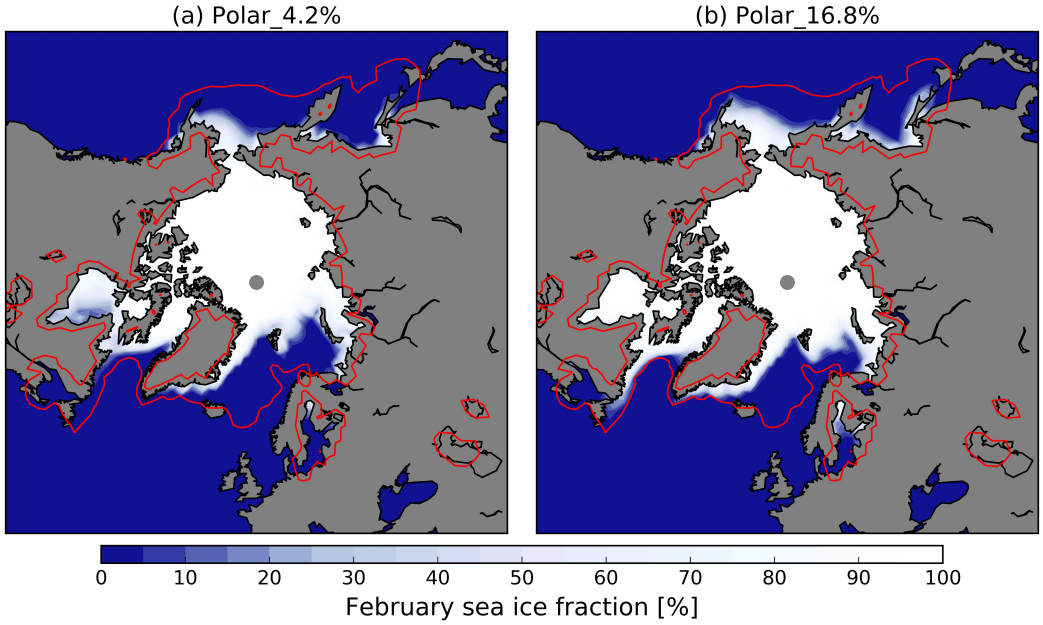

Figure 3.13: Arctic February mean sea ice fraction in the (a) Polar_4.2% and (b) Polar_16.8% climate engineered simulations. The red contour lines show the PI-Control sea ice edge (5% sea ice fraction) for comparison. Higher sea ice coverages are represented in white and lower values in light blue, and ocean is represented by dark blue colour.

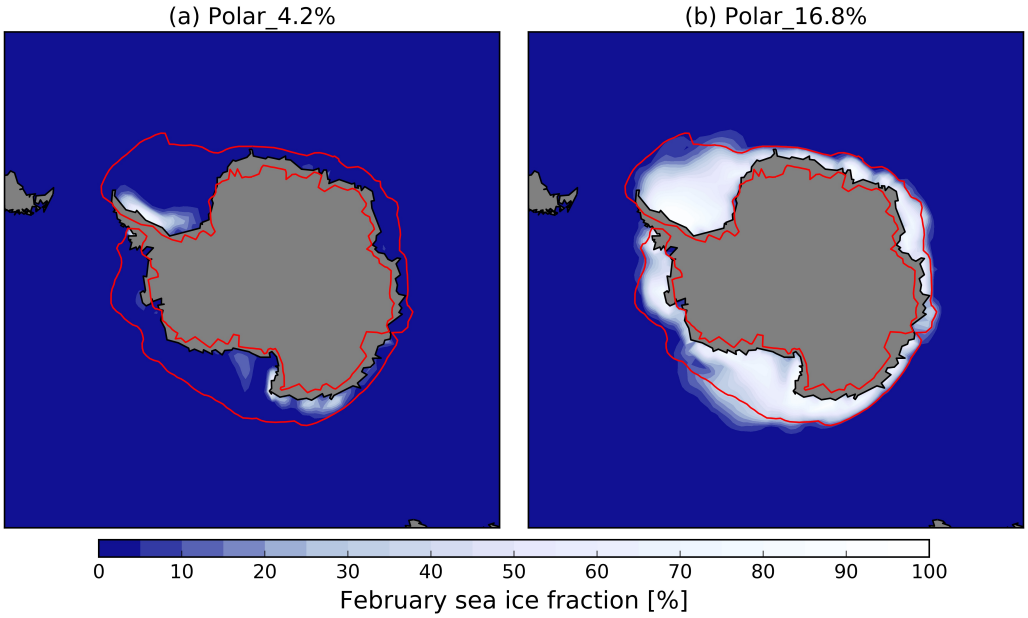

Figure 3.14: Antarctic February mean sea ice fraction in the (a) Polar_4.2% and (b) Polar_16.8% climate engineered simulations. The red contour lines show the PI-Control sea ice edge (5% sea ice fraction) for comparison. Higher sea ice coverages are represented in white and lower values in light blue, and ocean is represented by dark blue colour.

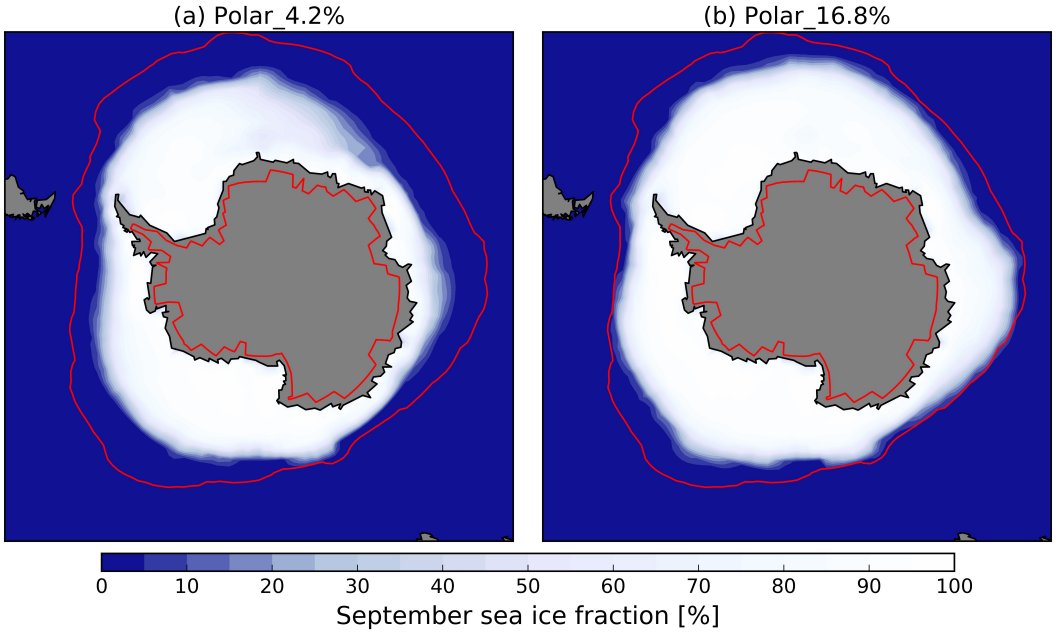

Figure 3.15: Antarctic September mean sea ice fraction in the (a) Polar_4.2% and (b) Polar_16.8% climate engineered simulations. The red contour lines show the PI-Control sea ice edge (5% sea ice fraction) for comparison. Higher sea ice coverages are represented in white and lower values in light blue, and ocean is represented by dark blue colour.

The patterns of the mean summer (September) Arctic sea-ice cover in the polar geoengineering simulations are shown in Figure 3.12 and the mean winter(February) Arctic sea ice cover are shown in Figure 3.13. The mean Antarctic summer (February) and winter (September) sea ice are shown in Figure 3.14 and Figure 3.15 respectively. The 4.2% reduction in solar radiation at the polar regions was not enough to bring the warming down to recover the sea ice as the high latitudes warm much more than the rest of the globe in the abrupt4×CO_2 simulation, although the Global_4.2% in insolation was able to bring the global mean surface temperature down to almost the pre-industrial state. The Polar_4.2 simulation was able to just preserved a small portion of the summer sea ice in the Central Arctic unlike the Global_4.2 simulation that recovered most of the sea ice. This is because the reduction was done only at the polar regions and the 4.2% was not enough to counteract the amplified warming in the region and the warming from

the other regions without solar reduction might also transport to the poles.

The annual average Arctic sea ice fraction is 80.7±2.3% (Table 3.3) compared to the condition in PI-Control and the annual average Antarctic sea ice fraction is 87.7±4.1% (Table 3.4) compared to the condition in PI-Control. The Polar_16.8 climate engineered simulation compensated most of the abrupt4×CO_2 warming in the polar regions to restored the substantially decreased in September sea ice extent closer to the PI-Control level (Figure 3.12b). The September mean sea ice in the Arctic is slightly lower than the condition in the PI-Control simulation. This is because the northern hemisphere suffers more warming from the atmospheric abrupt4×CO_2 than the rest of the globe. The reduction in solar radiation favours the summer sea ice but has a little impact on the winter sea ice since there is no sunlight during the winter season. From Figure 3.13, the sea ice extent in the Polar_4.2 and 16.8 looks almost similar unlike the summer sea ice in Figure 3.12 where the Polar_16.8 recovered almost all the September sea ice to the level of PI-Control simulation. This is because solar reduction is effective during summer when there is sunlight. Figure 3.14b shows more ice over the Ross sea and the Weddell sea. There is a slight decrease in West Antarctica sea ice but the sea ice in the East Antarctica is recovered. With the Polar_16.8 reduction in insolation, the ocean albedo will increase significantly leading to decreasing in shortwave absorption as the sea ice coverage is restored similar to the preindustrial condition and that will lead less latent heat release from the ocean to the atmosphere.

3.4 Statistical Tables

Simulation	Temperature (K)	Temperature difference (^{o}C)
PI-Control	285.2	-
Abrupt4×CO_2	289.9±0.13	4.7
Global_4.2	285.4±0.10	0.2
Polar_4.2	289.5±0.16	4.3
Polar_16.8	288.4±0.14	3.2

Table 3.1: Statistics of the annual mean surface air temperature changes in the 4×CO_2 and climate engineering cases relative to the PI-Control simulation.

Simulations	Change in Precipitation (%)
PI-Control	-
Abrupt4×CO_2	7.5±0.62
Global_4.2	-2.8±0.47
Polar_16.8	5.0±0.60

Table 3.2: Statistics of the annual mean precipitation changes in the 4×CO_2, Global_4.2 and Polar_16.8% climate engineering relative to the PI-Control simulation.

Simulation	Arctic sea ice (%)
PI-Control	-
Abrupt4×CO_2	44.0±2.9
Global_4.2	94.5±2.3
Polar_4.2	53.7±2.7
Polar_16.8	80.7±2.3

Table 3.3: Statistics of the annual mean Arctic sea ice changes in the 4×CO_2 and climate engineering cases relative to the PI-Control simulation.

Simulation	Antarctic sea ice (%)
PI-Control	-
Abrupt4×CO_2	35.0±3.7
Global_4.2	110.9±3.8
Polar_4.2	48.4±3.6
Polar_16.8	87.7±4.1

Table 3.4: Statistics of the annual mean Antarctic sea ice changes in the 4×CO_2 and climate engineering cases relative to the PI-Control simulation.

Tables (3.1, 3.2, 3.3, and 3.4) show that, the idealised global uniform 4.2% solar engineering where the sunlight was uniformly fractionally reduced brings the abrupt4×CO_2 climate more similar to the values of the PI-Control climate than to those of the polar simulations with respect to surface air temperature, precipitation and sea ice on a global mean basis.

Chapter 4

Discussion

Four model simulations were performed in this study to test for the effectiveness and feasibility of climate engineering using the solar radiation management approach. The results from the idealised CO_2 simulation suggests that continuing increase in atmospheric carbon dioxide (CO_2) concentration will have a profound influence on the climate system and lead the Earth energy budget out of balance. This increase in emissions will cause future climate extreme events on the globe, like extreme surface temperature and precipitation. Increases in the atmospheric CO_2 concentrations causes Earth to warm by trapping more heat mainly infrared radiation, emitted from the Earth's surface. Efforts to limit the climate change and its risks which require substantial and sustained reductions in greenhouse gas emissions to keep the global warming below 2°C as internationally agreed has become difficult and challenge as so little has been done so far and greenhouse gases (GHG) continue to increase. However, reducing the solar radiation or blocking the sunlight that strikes the Earth at the top of the atmosphere to compensate the atmospheric CO_2 concentrations has emerged as an alternative approach to manage or counteract climate change. Nevertheless, our solar climate engineering simulation results clearly show that Solar Radiation Management can be used to manage climate change and some of its adverse effects.

A large reduction in incoming sunlight, as simulated in the solar geoengineering experiments, would reduce the global-mean temperature and surface temperatures everywhere compared to the temperatures in the abrupt4×CO_2 simulation. The engineered simulation in which incoming solar radiation was reduced globally by 4.2% largely compensated the global warming from the quadrupling atmospheric CO_2, mostly from summer seasons. The winter warming, comparably, are less sensitive to solar geoengineering. Therefore, solar geoengineering could result in a world with weaker seasonality, especially those over higher latitudes. This somehow, could be beneficial for our society, sine we can have mild winter.

In addition, the 16.8% reduction in the polar regions largely reduce the warming caused by the quadrupled CO_2 concentration locally, especially during summer. This could help to reduce the risk of sea level rise caused by melting of polar ice sheets. Comparing the simulations, the regions with greatest reduction in the global-mean temperature and surface temperatures in the engineered climates are those regions which showed the greatest warming under the abrupt4×CO_2 conditions, that is, at high-latitudes where strong positive feedbacks act on temperature changes (*Kravitz et al.*, 2013). The reduction in solar radiation favours cooling in the tropics while CO_2 favours warming over the higher-latitude, because the strongest radiation is around the equator and reduction in radiative forcing from the quadrupled atmospheric CO_2 (*Govindasamy and Caldeira*, 2000). The residual warming found in some regions is in agreement with earlier studies (*Robock et al.*, 2008; *Ricke et al.*, 2010) which shown that the level of compensation will vary with residual changes larger in some regions than others. The most residual warming found at the polar regions during winter season, as solar reduction has little impact on the winter polar regions. The pattern in precipitation under the abrupt4×CO_2 simulation suggests that the global hydrological cycle will be stronger, causing 'dry get dryer and wet get wetter'. Besides, there is a general poleward shift of the precipitation pattern caused by poleward shift of the atmospheric circulation

(*Yang et al.*, 2022). The changes in global mean precipitation under the impact of global warming is associated with changes not only in precipitation intensity but also in precipitation frequency (*Chou and Lan*, 2012). We find that solar radiation management is able to reduce the intensity of hydrological cycle, even possible to cause drought if too much solar radiation is reduced to offset mean global warming. The reduction in precipitation is as a result of the fundamental difference between the effects of the CO_2 forcing and the solar forcing on the thermal structure of the atmosphere (*Cao et al.*, 2015a). The absorption of long wave radiation by increased atmospheric CO_2 increases the vertical stability of the atmosphere, suppressing convection activities and precipitation in the absence of surface temperature changes (*Cao et al.*, 2015b). The atmosphere is more transparent to the solar radiation than the CO_2 forcing. With no difference in surface temperature, the solar irradiance change would have much smaller consequence on the vertical stability of the atmosphere and would cause reduction in precipitation due to CO_2 induced stability changes in the atmosphere. Using climate engineering to restore global mean surface temperature to the preindustrial climate state would result in a decrease in global precipitation. There should be residual warming to restore or maintain global precipitation using solar engineering.

Globally uniform 4.2% solar reduction causes stronger residual warming over land than that over the ocean. Due to the hemisphere asymmetric of land-sea distribution, this leads to anomaly of hemisphere temperature difference, which cause a meridional shift of the Intertropical Convergence Zone and the associated low-latitude precipitation. More specifically, more residual warming over the Northern Hemisphere due to more land coverage, leads to a northward shift of the Intertropical Convergence Zone. The simulated results demonstrated that solar geoengineering could be effective at preventing the Arctic and Antarctic sea ice loss from carbon dioxide (CO_2) emission. Sea ice is an integral part of the Arctic Ocean. The Arctic sea ice cover is one of the most prominent indicators of change

in the Arctic. Several climate models have shown significant downward trend in sea ice extent through the 21st Century *Stroeve et al.* (2007, 2012); *Eisenman et al.* (2011); *Xia et al.* (2014); *Johannessen et al.* (2004), as the planet warms in response to increasing in greenhouse gases concentrations with the summer minimum ice extent declining faster than the winter maximum. September is typically when sea ice reaches its minimum thickness and extent, when the area covered by ice is roughly half the size of the winter maximum. The amount of sea ice changes throughout the year as a consequence of the solar heating or warming the polar regions receive. Summer sea ice extent is declining increasingly fast and according to *Krishfield et al.* (2014), the thick perennial ice cover has now been replaced by a thinner first year ice. As sea-ice extent decreases during summer, more solar radiation is absorbed by the increased ocean area, heating the upper level of the ocean and delaying the onset of freeze-up and slowing ice growth. Most of the changes in sea ice cover are driven by anthropogenic warming from increasing atmospheric greenhouse gas concentrations in the atmosphere as shown in this study and amplified by internal variabilities (*Notz and Stroeve*, 2016). Observations have shown that sea level is rising and will continue to rise if the ice sheets fall apart rapidly. The engineered simulations are able to prevent and restored most of the sea ice, most especially the summer sea ice extent. Although, restoring September sea ice extent similar to the PI-Control levels in a $4\times CO_2$ atmosphere would require high percentage of reduction of insolation over the 60 degrees North and South poles of the earth.

Several modelling and experimental studies have demonstrated that solar geoengineering with global uniformly reduction can bring the global surface temperature similar to the preindustrial conditions (*Govindasamy and Caldeira*, 2000; *Govindasamy et al.*, 2002, 2003; *Ban-Weiss and Caldeira*, 2010; *MacMartin et al.*, 2014; *Caldeira and Wood*, 2008; *Kravitz et al.*, 2013). In this study, AWI-ESM was used to test for the solar geoengineering and the results found in this study are in

relation with the previous studies. Our model simulations also imply that solar geoengineering can reduce the global surface temperature to the levels of preindustrial with proper reduction in solar radiation at TOA.

In contrast to the fact that solar geoengineering approach is aimed at reducing climate risk, implementation of it could also introduce other environmental harmful side effects and new risks such as ocean acidification due to very high CO_2 concentration in the atmosphere, solar dimming, changes in rainfall with risk of drought and heavy rainfall. It will also have impact on regional climate change, part of the regions would have to suffers the solar blocking, like the 16.8% polar experiments, which may have a few hours dark time and may not be comfortable for the local people. Nevertheless, solar geoengineering could also offer environmental benefits such as increasing winter temperatures locally which could be of benefit to the local people and also block harmful UV radiation (*Teller et al.*, 2003).

Chapter 5

Conclusion and Outlook

Increase in atmospheric carbon dioxide (CO_2) concentration have had a profound influence on the climate system and will continue to increase and lead the Earth energy budget out of balance. Global mean surface temperatures will continue to rise without a proper intervention on the climate. In this study, we have used highly idealised simulations to test and analyse the impacts of abruptly $4\times CO_2$ concentration on the climate and also evaluated the feasibility and impacts of solar geoengineering on $4\times CO_2$ on global and regional climate. The $4\times CO_2$ caused global mean surface air temperature raise and radiative imbalance at the TOA. The $4\times CO_2$ shows a global mean surface air temperature raise with strongest positive anomalies in the high latitudes and over the land. Again, the $4\times CO_2$ shows a significant increase in global mean precipitation over many parts of the globe, but with a strong spatial inhomogeneous. It reduced the Arctic and the Antarctic annual mean sea ice fraction by 56.0% and 65.0% respectively, relative to the PI-Control condition.

The globally uniform 4.2% solar climate engineering compensates the global mean surface warming in the abrupt$4\times CO_2$ simulation with residual cooling over low-latitude summer and residual warming high latitude winter and land. Further, the globally reduction significantly cause an overall reduction in global hydrological

cycle and hence reduces precipitation of about (2.8±0.47%) compared to the global precipitation in the PI-Control simulation, although, with small positive and negative anomalies over different parts of the globe. Solar reduction is most efficient to bring down the summer warming over low-latitudes due to stronger solar radiation is located during summer at low-latitude. The remain winter warming may be beneficial for our society, since we can have mild winter. Using an alternative strategy, polar solar reduction can largely offset the summer polar warming to prevent sea ice loss and disintegration of the ice sheets. However, solar reduction could lead to drought. As the GHG warming could cause warmer atmosphere, solar reduction produces less evaporation. Solar geoengineering will also reduce the global mean precipitation.

Our idealised model simulation results indicate that solar climate engineering by putting sun-shields or installing giant mirrors in space to reflect the incoming solar radiation (sunlight) could significantly diminish some adverse effects of increasing CO_2 emissions on global surface air temperature, precipitation and sea ice and ice sheets. However, solar reduction cannot simultaneously reverse all adverse effects of CO_2 induced changes in both global mean temperature and global mean precipitation.

Further studies should consider the transient responses of the climate system, interactive ice sheets and the potential effects and risks of solar climate engineering on the climate. It might be interested to also consider solar reduction in the subtropical region, as the climatology maximum averaged solar radiation locates at the lower latitudes.

Recommendations

The following recommendations are suggested for future studies in order to improve our understanding in climate engineering particularly Solar Radiation Management scenario and have much detailed information on it.

- In this study we used idealised method for the simulations. But, in reality, more realistic experiment should be conducted with actual solar eclipse driven by satellite orbit to precisely access the feasibility and effectiveness of solar geoengineering.
- Much attention should be on polar solar geoengineering since very less people are living in the region and might cause less effect on the global population and less cost as compared to the global geoengineering.
- Other greenhouse gases must be considered in the future work since only CO_2 emissions was considered in this study.
- Climate engineering experiments should use more detailed scenarios in future to test for its effectiveness.

Acronyms

AWI Alfred Wegener Institute

CDR Carbon Dioxide Removal

DJF December-January-February

ECHAM6 European Center-Hamburg Model, Version 6

ECS Equilibrium Climate Sensitivity

ERF Effective Radiative Forcing

ESM Earth System Model

FESOM Finite Element Sea-Ice Ocean Mode

GHG Green-House Gases

IPCC Intergovernmental Panel on Climate Change

JJA June-July-August

NH Northern Hemisphere

SH Southern Hemisphere

SRM Solar Radiation Management

TOA Top of Atmosphere

UN United Nations

Bibliography

Arora, V., J. Scinocca, G. Boer, J. Christian, K. Denman, G. Flato, V. Kharin, W. Lee, and W. Merryfield (2011), Carbon emission limits required to satisfy future representative concentration pathways of greenhouse gases, *Geophysical Research Letters*, *38*(5), doi:10.1029/2010GL046270.

Bal, P. K., R. Pathak, S. K. Mishra, and S. Sahany (2019), Effects of global warming and solar geoengineering on precipitation seasonality, *Environmental Research Letters*, *14*(3), 034,011, doi:10.1088/1748-9326/aafc7d.

Bala, G. (2009), Problems with geoengineering schemes to combat climate change, *Current Science*, pp. 41–48, http://www.jstor.org/stable/24104726.

Bala, G., P. Duffy, and K. Taylor (2008), Impact of geoengineering schemes on the global hydrological cycle, *Proceedings of the National Academy of Sciences*, *105*(22), 7664–7669, doi:10.1073/pnas.0711648105.

Ban-Weiss, G. A., and K. Caldeira (2010), Geoengineering as an optimization problem, *Environmental Research Letters*, *5*(3), 034,009, doi:10.1088/1748-9326/5/3/034009.

Block, K., and T. Mauritsen (2013), Forcing and feedback in the mpi-esm-lr coupled model under abruptly quadrupled co2, *Journal of Advances in Modeling Earth Systems*, *5*(4), 676–691, doi:10.1002/jame.20041.

Brierley, C. M., A. Zhao, S. P. Harrison, P. Braconnot, C. J. R. Williams, D. J. R. Thornalley, X. Shi, J.-Y. Peterschmitt, R. Ohgaito, D. S. Kaufman, M. Kageyama, J. C. Hargreaves, M. P. Erb, J. Emile-Geay, R. D'Agostino, D. Chandan, M. Carré, P. Bartlein, W. Zheng, Z. Zhang, Q. Zhang, H. Yang, E. M. Volodin, R. A. Tomas, C. Routson, W. R. Peltier, B. Otto-Bliesner, P. A. Morozova, N. P. McKay, G. Lohmann, A. N. LeGrande, C. Guo, J. Cao, E. Brady, J. D. Annan, and A. Abe-Ouchi (2020), Large-scale features and evaluation of the PMIP4-CMIP6 midHolocene simulations, *Climate of the Past*, *16*(5), 1847–1872, doi:10.5194/cp-16-1847-2020.

Caldeira, K., and L. Wood (2008), Global and arctic climate engineering: numerical model studies, *Philosophical Transactions of the Royal Society A: Mathematical, Physical and Engineering Sciences*, *366*(1882), 4039–4056, https://doi.org/10.1098/rsta.2008.0132.

Caldeira, K., G. Bala, and L. Cao (2013), The science of geoengineering, *Annual Review of Earth and Planetary Sciences*, *41*, doi:10.1146/annurev-earth-042711-105548, https://doi.org/10.1146/annurev-earth-042711-105548.

Cao, L., G. Bala, M. Zheng, and K. Caldeira (2015a), Fast and slow climate responses to co2 and solar forcing: A linear multivariate regression model characterizing transient climate change, *Journal of Geophysical Research: Atmospheres*, *120*(23), 12–037, doi:10.1002/2015JD023901.

Cao, L., C.-C. Gao, and L.-Y. Zhao (2015b), Geoengineering: Basic science and ongoing research efforts in china, *Advances in climate change research*, *6*(3-4), 188–196, doi:10.1016/j.accre.2015.11.002.

Chou, C., and C.-W. Lan (2012), Changes in the annual range of precipita-

tion under global warming, *Journal of Climate*, *25*(1), 222–235, doi:10.1175/JCLI-D-11-00097.1.

Council, N. R. (2015), *Climate intervention: Carbon dioxide removal and reliable sequestration*, National Academies Press, doi:10.17226/18805.

Crutzen, P. J. (2006), Albedo enhancement by stratospheric sulfur injections: A contribution to resolve a policy dilemma?, *Climatic change*, *77*(3-4), 211, doi:10.1007/s10584-006-9101-y.

Eisenman, I., T. Schneider, D. S. Battisti, and C. M. Bitz (2011), Consistent changes in the sea ice seasonal cycle in response to global warming, *Journal of Climate*, *24*(20), 5325–5335, doi:10.1175/2011JCLI4051.1.

Gent, P. R., G. Danabasoglu, L. J. Donner, M. M. Holland, E. C. Hunke, S. R. Jayne, D. M. Lawrence, R. B. Neale, P. J. Rasch, M. Vertenstein, P. H. Worley, Z.-L. Yang, and M. Zhang (2011), The community climate system model version 4, *Journal of climate*, *24*(19), 4973–4991, doi:10.1175/2011JCLI4083.1.

Govindasamy, B., and K. Caldeira (2000), Geoengineering Earth's radiation balance to mitigate CO2-induced climate change, *Geophysical Research Letters*, *27*(14), 2141–2144, doi:10.1029/1999GL006086.

Govindasamy, B., S. Thompson, P. B. Duffy, K. Caldeira, and C. Delire (2002), Impact of geoengineering schemes on the terrestrial biosphere, *Geophysical Research Letters*, *29*(22), 18–1, doi:10.1029/2002GL015911.

Govindasamy, B., K. Caldeira, and P. Duffy (2003), Geoengineering Earth's radiation balance to mitigate climate change from a quadrupling of CO2, *Global and Planetary Change*, *37*(1-2), 157–168, doi:10.1016/S0921-8181(02)00195-9.

Gregory, J., W. Ingram, M. Palmer, G. Jones, P. Stott, R. Thorpe, J. Lowe, T. Johns, and K. Williams (2004), A new method for diagnosing radia-

tive forcing and climate sensitivity, *Geophysical research letters*, *31*(3), doi: 10.1029/2003GL018747.

Hu, Y., and Q. Fu (2007), Observed poleward expansion of the hadley circulation since 1979, *Atmospheric Chemistry and Physics*, *7*(19), 5229–5236.

Irvine, P. J., B. Kravitz, M. G. Lawrence, and H. Muri (2016), An overview of the earth system science of solar geoengineering, *Wiley Interdisciplinary Reviews: Climate Change*, *7*(6), 815–833, doi:10.1002/wcc.423.

Ji, D., L. Wang, J. Feng, Q. Wu, H. Cheng, Q. Zhang, J. Yang, W. Dong, Y. Dai, D. Gong, R.-H. Zhang, X. Wang, J. Liu, J. C. Moore, D. Chen, and M. Zhou (2014), Description and basic evaluation of beijing normal university earth system model (bnu-esm) version 1, *Geoscientific Model Development*, *7*(5), 2039–2064, doi:10.5194/gmd-7-2039-2014.

Johannessen, O. M., L. Bengtsson, M. W. Miles, S. I. Kuzmina, V. A. Semenov, G. V. Alekseev, A. P. Nagurnyi, V. F. Zakharov, L. P. Bobylev, L. H. Pettersson, K. Hasselmann, and H. P. Cattle (2004), Arctic climate change: observed and modelled temperature and sea-ice variability, *Tellus A: Dynamic Meteorology and Oceanography*, *56*(4), 328–341, doi:10.3402/tellusa.v56i4.14418.

Kageyama, M., S. P. Harrison, M.-L. Kapsch, M. Löfverström, J. M. Lora, U. Mikolajewicz, S. Sherriff-Tadano, T. Vadsaria, A. Abe-Ouchi, N. Bouttes, D. Chandan, A. N. LeGrande, F. Lhardy, G. Lohmann, P. A. Morozova, R. Ohgaito, W. R. Peltier, A. Quiquet, D. M. Roche, X. Shi, A. Schmittner, J. E. Tierney, and E. Volodin (2020), The PMIP4-CMIP6 Last Glacial Maximum experiments: preliminary results and comparison with the PMIP3-CMIP5 simulations, *Climate of the Past Discussions*, *in review, 2020*, 1–37, doi:10.5194/cp-2019-169.

Kelley, M., G. A. Schmidt, L. S. Nazarenko, S. E. Bauer, R. Ruedy, G. L. Russell, A. S. Ackerman, I. Aleinov, M. Bauer, R. Bleck, V. Canuto, G. Cesana, Y. Cheng, T. L. Clune, D. Kim, A. A. Lacis, A. Leboissetier, A. N. LeGrande, K. K. Lo, J. Marshall, E. E. Matthews, S. McDermid, K. Mezuman, R. L. Miller, L. T. Murray, V. Oinas, C. Obre, C. P. García-Pando, J. P. Perlwitz, M. J. Puma, D. Rind, A. Romanou, D. T. Shindell, S. Sun, N. Tausnev, K. Tsigaridis, G. Tselioudis, E. Weng, J. Wu, and M.-S. Yao (2020), Giss-e2. 1: Configurations and climatology, *Journal of Advances in Modeling Earth Systems*, *12*(8), e2019MS002,025, doi:10.1029/2019MS002025.

Kravitz, B., K. Caldeira, O. Boucher, A. Robock, P. J. Rasch, K. Alterskjær, D. B. Karam, J. N. Cole, C. L. Curry, J. M. Haywood, P. J. Irvine, D. Ji, A. Jones, J. E. Kristjánsson, D. J. Lunt, J. C. Moore, U. Niemeier, H. Schmidt, M. Schulz, B. Singh, S. Tilmes, S. Watanabe, S. Yang, and J. Yoon (2013), Climate model response from the geoengineering model intercomparison project (GeoMIP), *Journal of Geophysical Research: Atmospheres*, *118*(15), 8320–8332, https://hal.archives-ouvertes.fr/hal-01091232.

Kravitz, B., D. G. MacMartin, D. Visioni, O. Boucher, J. N. Cole, J. Haywood, A. Jones, T. Lurton, P. Nabat, U. Niemeier, A. Robock, R. Séférian, and S. Tilmes (2021), Comparing different generations of idealized solar geoengineering simulations in the geoengineering model intercomparison project (geomip), *Atmospheric Chemistry and Physics*, *21*(6), 4231–4247, doi:10.5194/ACP-21-4231-2021.

Krishfield, R. A., A. Proshutinsky, K. Tateyama, W. J. Williams, E. C. Carmack, F. A. McLaughlin, and M.-L. Timmermans (2014), Deterioration of perennial sea ice in the beaufort gyre from 2003 to 2012 and its impact on the oceanic freshwater cycle, *Journal of Geophysical Research: Oceans*, *119*(2), 1271–1305, doi:10.1002/2013JC008999.

Lohmann, G. (2020), Temperatures from energy balance models: the effective heat capacity matters, *Earth System Dynamics*, *11*(4), 1195–1208, doi:10.5194/esd-11-1195-2020, https://doi.org/10.5194/esd-11-1195-2020.

Lohmann, G., M. Butzin, N. Eissner, X. Shi, and C. Stepanek (2020), Abrupt climate and weather changes across time scales, *Paleoceanography and Paleoclimatology*, *35*(9), e2019PA003,782, doi:10.1029/2019PA003782, Special Section AGU Grand Challenges in the Earth and Space Sciences.

Lu, J., G. A. Vecchi, and T. Reichler (2007), Expansion of the hadley cell under global warming, *Geophysical Research Letters*, *34*(6), doi:10.1029/2006GL028443.

Lurton, T., Y. Balkanski, V. Bastrikov, S. Bekki, L. Bopp, P. Braconnot, P. Brockmann, P. Cadule, C. Contoux, A. Cozic, D. Cugnet, J.-L. Dufresne, C. Éthé, M.-A. Foujols, J. Ghattas, D. Hauglustaine, R.-M. Hu, M. Kageyama, M. Khodri, N. Lebas, G. Levavasseur, M. Marchand, C. Ottlé, P. Peylin, A. Sima, S. Szopa, R. Thiéblemont, N. Vuichard, and O. Boucher (2020), Implementation of the CMIP6 forcing data in the IPSL-CM6A-LR model, *Journal of Advances in Modeling Earth Systems*, *12*(4), e2019MS001,940, doi:10.1029/2019MS001940.

MacMartin, D. G., B. Kravitz, and D. W. Keith (2014), Geoengineering: The world's largest control problem, in *2014 American Control Conference*, pp. 2401–2406, IEEE, doi:10.1109/ACC.2014.6858658.

MacMartin, D. G., K. L. Ricke, and D. W. Keith (2018), Solar geoengineering as part of an overall strategy for meeting the 1.5 C paris target, *Philosophical Transactions of the Royal Society A: Mathematical, Physical and Engineering Sciences*, *376*(2119), 20160,454, doi:10.1098/rsta.2016.0454.

McClellan, J., D. W. Keith, and J. Apt (2012), Cost analysis of stratospheric

albedo modification delivery systems, *Environmental Research Letters*, *7*(3), 034,019, doi:10.1088/1748-9326/7/3/034019.

Meehl, G. A., C. A. Senior, V. Eyring, G. Flato, J.-F. Lamarque, R. J. Stouffer, K. E. Taylor, and M. Schlund (2020), Context for interpreting equilibrium climate sensitivity and transient climate response from the cmip6 earth system models, *Science Advances*, *6*(26), eaba1981, doi:10.1126/sciadv.aba1981.

Notz, D., and J. Stroeve (2016), Observed arctic sea-ice loss directly follows anthropogenic co2 emission, *Science*, *354*(6313), 747–750, doi:10.1126/science.aag2345.

Ricke, K. L., M. G. Morgan, and M. R. Allen (2010), Regional climate response to solar-radiation management, *Nature Geoscience*, *3*(8), 537–541, https://doi.org/10.1038/ngeo915.

Robock, A., L. Oman, and G. L. Stenchikov (2008), Regional climate responses to geoengineering with tropical and arctic so2 injections, *Journal of Geophysical Research: Atmospheres*, *113*(D16), https://doi.org/10.1029/2008JD010050.

Russotto, R. D., and T. P. Ackerman (2018), Changes in clouds and thermodynamics under solar geoengineering and implications for required solar reduction, *Atmospheric Chemistry and Physics*, *18*(16), 11,905–11,925, https://doi.org/10.5194/acp-18-11905-2018.

Shi, X., G. Lohmann, D. Sidorenko, and H. Yang (2020), Early-Holocene simulations using different forcings and resolutions in AWI-ESM, *The Holocene*, *30*(7), 996–1015, doi:10.1177/0959683620908634.

Sidorenko, D., H. Goessling, N. Koldunov, P. Scholz, S. Danilov, D. Barbi, W. Cabos, O. Gurses, S. Harig, C. Hinrichs, S. Juricke, G. Lohmann, M. Losch, L. Mu, T. Rackow, N. Rakowsky, D. Sein, T. Semmler, X. Shi, C. Stepanek,

J. Streffing, Q. Wang, C. Wekerle, H. Yang, and T. Jung (2019), Evaluation of FESOM2. 0 coupled to ECHAM6. 3: preindustrial and HighResMIP simulations, *Journal of Advances in Modeling Earth Systems*, *11*(11), 3794–3815, doi:10.1029/2019MS001696.

Stocker, T. F., D. Qin, G.-K. Plattner, L. V. Alexander, S. K. Allen, N. L. Bindoff, F.-M. Bréon, J. A. Church, U. Cubasch, S. Emori, P. Forster, P. Friedlingstein, N. Gillett, J. M. Gregory, D. L. Hartmann, E. Jansen, B. Kirtman, R. Knutti, K. Krishna Kumar, P. Lemke, J. Marotzke, V. Masson-Delmotte, G. A. Meehl, I. I. Mokhov, S. Piao, V. Ramaswamy, D. Randall, M. Rhein, M. Rojas, C. Sabine, D. Shindell, L. D. Talley, D. G. Vaughan, and S.-P. Xie (2013), Technical summary, in *Climate change 2013: the physical science basis. Contribution of Working Group I to the Fifth Assessment Report of the Intergovernmental Panel on Climate Change*, edited by T. F. Stocker, D. Qin, G.-K. Plattner, M. Tignor, S. K. Allen, J. Doschung, A. Nauels, Y. Xia, V. Bex, and P. M. Midgley, pp. 33–115, Cambridge University Press, Cambridge, UK, doi:10.1017/CBO9781107415324.005.

Stroeve, J., and D. Notz (2018), Changing state of arctic sea ice across all seasons, *Environmental Research Letters*, *13*(10), 103,001, doi:10.1088/1748-9326/aade56, https://doi.org/10.1088/1748-9326/aade56.

Stroeve, J., M. M. Holland, W. Meier, T. Scambos, and M. Serreze (2007), Arctic sea ice decline: Faster than forecast, *Geophysical research letters*, *34*(9), https://doi.org/10.1029/2007GL029703.

Stroeve, J. C., M. C. Serreze, M. M. Holland, J. E. Kay, J. Malanik, and A. P. Barrett (2012), The arctic's rapidly shrinking sea ice cover: a research synthesis, *Climatic change*, *110*(3), 1005–1027, https://doi.org/10.1007/s10584-011-0101-1.

Teller, E., R. Hyde, M. Ishikawa, J. Nuckolls, and L. Wood (2003), Active stabilization of climate: inexpensive, low-risk, near-term options for preventing global warming and ice ages via technologically varied solar radiative forcing, *University of California Lawrence Livermore National Laboratory*.

Tietsche, S., D. Notz, J. Jungclaus, and J. Marotzke (2011), Recovery mechanisms of arctic summer sea ice, *Geophysical Research Letters*, *38*(2), doi: 10.1029/2010GL045698.

Walsh, J. E. (2014), Intensified warming of the arctic: Causes and impacts on middle latitudes, *Global and Planetary Change*, *117*, 52–63, doi:10.1016/j.gloplacha.2014.03.003, https://ui.adsabs.harvard.edu/abs/2014GPC...117...52W, Provided by the SAO/NASA Astrophysics Data System.

Xia, W., H. Xie, and C. Ke (2014), Assessing trend and variation of arctic sea-ice extent during 1979–2012 from a latitude perspective of ice edge, *Polar Research*, *33*(1), 21,249, https://doi.org/10.3402/polar.v33.21249.

Yang, H., G. Lohmann, U. Krebs-Kanzow, M. Ionita, X. Shi, D. Sidorenko, X. Gong, X. Chen, and E. J. Gowan (2020a), Poleward shift of the major ocean gyres detected in a warming climate, *Geophysical Research Letters*, *47*(5), e2019GL085,868, doi:10.1029/2019GL085868.

Yang, H., G. Lohmann, J. Lu, E. J. Gowan, X. Shi, J. Liu, and Q. Wang (2020b), Tropical expansion driven by poleward advancing midlatitude meridional temperature gradients, *Journal of Geophysical Research: Atmospheres*, *125*(16), e2020JD033,158, doi:10.1029/2020JD033158.

Yang, H., J. Lu, Q. Wang, X. Shi, and G. Lohmann (2022), Decoding the dynamic of poleward shifting climate zones using aqua-planet model simulation, *Climate Dynamics*, doi:10.1007/s00382-021-06112-0.

Zhang, Z., J. C. Moore, D. Huisingh, and Y. Zhao (2015), Review of geoengineering approaches to mitigating climate change, *Journal of Cleaner Production*, *103*, 898–907, doi:10.1016/j.jclepro.2014.09.076.

Appendices

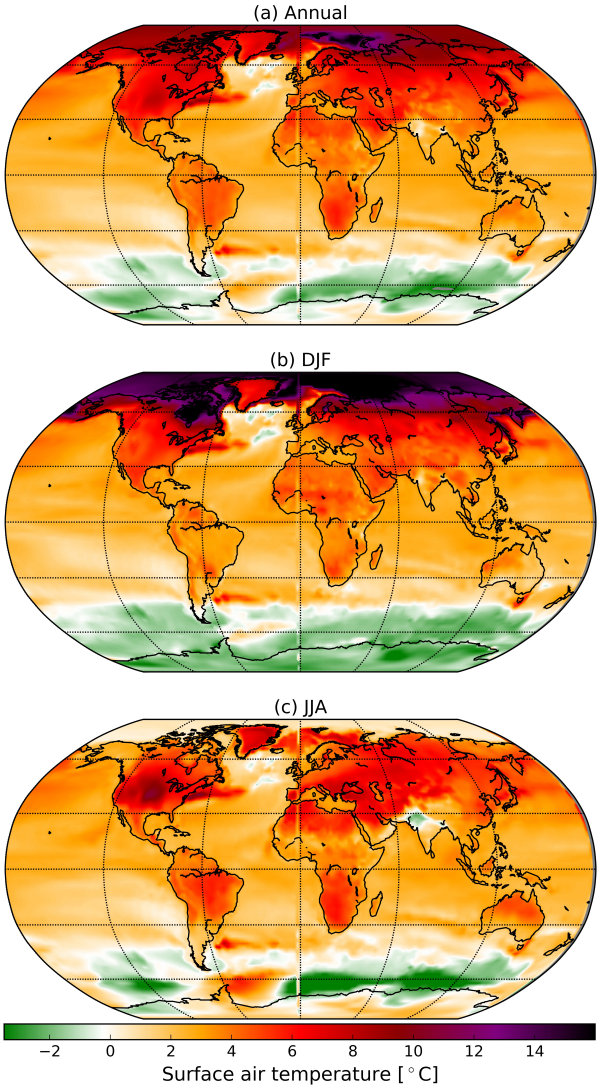

Figure 5.1: Global surface air temperature anomalies for (a) Annual, (b) December-January-February (DJF) and (c) June-July-August (JJA) average relative to PI control simulation in the Southern_16.8% simulation in Southern Hemisphere over 45°C, showing the changes in the surface temperature from the abrupt $4\times CO_2$.